Atmos. Chem. Phys. Discuss., 14, 27663–27729, 2014
www.atmos-chem-phys-discuss.net/14/27663/2014/
doi:10.5194/acpd-14-27663-2014

Atmospheric Chemistry and Physics Discussions

A new model of the global biogeochemical cycle of carbonyl sulfide – Part 2: Use of ocs to constrain gross primary productivity of current vegetation models

T. Launois, P. Peylin, S. Belviso, and B. Poulter

Laboratoire des Sciences du Climat et de l'Environnement (LSCE), IPSL, CEA, CNRS, UVSQ, CE Saclay, Bât 701 L'Orme des Merisiers, 91191, Gif-sur-Yvette, France

Received: 3 September 2014 – Accepted: 13 October 2014 – Published: 5 November 2014

Correspondence to: T. Launois (thomas.launois@lsce.ipsl.fr)

Published by Copernicus Publications on behalf of the European Geosciences Union.

Abstract

Clear analogies between carbonyl sulfide (OCS) and carbon dioxide (CO_2) diffusion pathways through leaves have been revealed by experimental studies with plant uptake playing an important role for the atmospheric budget of both species. Here we use atmospheric OCS to evaluate the gross primary production (GPP) of three dynamic global vegetation models (LPJ, NCAR-CLM4 and ORCHIDEE). Vegetation uptake of OCS is modeled as a linear function of GPP and LRU, the ratio of OCS to CO_2 deposition velocities to plants. New parameterizations for the non-photosynthetic sinks (oxic soils, atmospheric oxidation) and biogenic sources (oceans and anoxic soils) of OCS are also provided. Despite new large oceanic emissions, global OCS budgets created with each vegetation model show exceeding sinks by several hundreds of $Gg\,S\,yr^{-1}$. An inversion of the surface fluxes (optimization of a global scalar which accounts for flux uncertainties) led to balanced OCS global budgets, as atmospheric measurements suggest, mainly by drastic reduction (−30 %) of soil and vegetation uptakes.

The amplitude of variations in atmospheric OCS mixing ratios is mainly dictated by the vegetation sink over the Northern Hemisphere. This allows for bias recognition in the GPP representations of the three selected models. Main bias patterns are (i) the terrestrial GPP of ORCHIDEE at high Northern latitudes is currently over-estimated, (ii) the seasonal variations of the GPP are out of phase in the NCAR-CLM4 model, showing a maximum carbon uptake too early in spring in the northernmost ecosystems, (iii) the overall amplitude of the seasonal variations of GPP in NCAR-CLM4 is too small, and (iv) for the LPJ model, the GPP is slightly out of phase for northernmost ecosystems and the respiration fluxes might be too large in summer in the Northern Hemisphere.

ACPD
14, 27663–27729, 2014

1 Introduction

The continental biosphere is an integral component of the climate system, and of the carbon and water cycles: it has absorbed about a quarter of the CO_2 released into the atmosphere by anthropogenic activities (Working Group I Contribution to the IPCC Fifth Assessment Report (AR5), Climate Change 2013: The Physical Science Basis) and it modulates the water balance over land. The functioning of the terrestrial biosphere can be heavily affected by climate change in particular by the assumed increase in climate extreme events (Grace and Rayment, 2000; Piovesan and Adams, 2000; Ciais et al., 2005; Schaphoff et al., 2006; Poulter et al., 2014). These events have the potential to reduce photosynthesis or increase ecosystem respiration (e.g., the impact of the European heatwave in 2003 addressed by Ciais et al., 2005). Quantifying carbon storage by ecosystems and predicting their sensitivity to future climate change relies heavily on our ability to diagnose the separate fluxes of photosynthesis and respiration at different scales. Terrestrial gross primary productivity (GPP) remains poorly constrained at global scales, with recent estimates differing by 30–40 $PgC\,yr^{-1}$ (Beer et al., 2010; Sitch et al., 2014).

The net flux exchanged by an ecosystem (NEE) can be measured continuously by the eddy-correlation technique at site level. However, GPP is not directly measurable. Indirect approaches have been proposed to estimate the biospheric gross fluxes (GPP and respiration): for instance, by using differences between nighttime and daytime NEE measurements (Reichstein et al., 2005; Lasslop et al., 2010) or combining different tracers including stable isotopologues of CO_2 (^{13}C and ^{18}O) (Knohl et al., 2005; Scartazza et al., 2004; Wingate et al., 2010). However, the underlying hypotheses in these approaches impose limitations, especially the poor knowledge of the isotopic signatures of different gross fluxes and their temporal variations when using ^{13}C and ^{18}O data. Moreover, when local measurements are used to calibrate or compare with large-scale estimates, the process of extrapolation creates further uncertainty.

ACPD
14, 27663–27729, 2014

Carbonyl sulfide (OCS) is now measured at several atmospheric monitoring stations, and its use as a tracer promises to bring new constraints on the gross fluxes of CO_2. The concept is based on the absorption of OCS by vegetation being directly linked to that of CO_2. Although there is compelling evidence that OCS uptake at the leaf scale is essentially a one-way process (Sandoval-Soto, 2005; Seibt et al., 2010), the link between OCS absorption and photosynthesis is more complex than expected because OCS absorption also takes place during the night and because the leaf relative uptake ratios of OCS and CO_2 during photosynthesis vary with light level (Maseyk et al., 2014). At larger scales (ecosystems, regions or continents), the link between OCS absorption and photosynthesis is also weaker than expected because soils take up atmospheric OCS too and can turn from a net sink to a net source, depending on whether or not they are saturated. If atmospheric OCS data are to be used to constraint fluxes in global modeling studies, there is no other option than to characterize the spatio-temporal variations in sources and sinks of this gas (Kettle et al., 2002; Suntharalingam et al., 2008; Berry et al., 2013).

Atmospheric records of OCS mixing ratios exhibit clear seasonal variations. Maximal and minimal values for OCS concentrations are observed in winter and summer, respectively, and the seasonal variations of OCS are highly correlated with those of CO_2 (Montzka et al., 2004).

Here, we used OCS to constrain the annual, seasonal and spatial variations of GPP of three dynamic global vegetation models (DGVMs): LPJ (Sitch et al., 2003), NCAR-CLM4 (hereafter referred to as CLM4CN) (Bonan and Levis, 2010; Lawrence et al., 2011), and ORCHIDEE (hereafter referred to as ORC) (Krinner et al., 2005). These DGVMs exhibit contrasting global photosynthetic carbon fluxes (120, 130 and 160 $Pg\,C\,yr^{-1}$, respectively). The differences in GPP involve not only the annual global total but also the phase and amplitude of the seasonal variations. All three tested DGVMs were chosen according to the results of the TRENDY experiment, which compared trends in global and regional CO_2 fluxes over the last two decades (TRENDY experiment, Sitch et al., 2014). For that, we have modeled the vegetation OCS sink

ACPD
14, 27663–27729, 2014

as proportional to GPP and the leaf relative uptake (LRU), where LRUs were taken from the inventory of Seibt et al. (2010), together with new parameterizations of the non-photosynthetic sinks of OCS (oxic soils and atmospheric oxidation) and of its biogenic emissions (from oceans and anoxic soils). To evaluate our current understanding and representation accuracy of the OCS biogeochemical cycle and quantify the relative impact of each surface flux, we transported those fluxes using the atmospheric LMDz transport model and compared simulated OCS atmospheric concentrations to observations from a database assembled by NOAA/ESRL. In the next step, we defined uncertainties associated with each surface flux and optimized these fluxes with an inverse modeling approach to minimize the difference in OCS atmospheric concentrations between simulations and observations.

With the results of these simulations, we successively investigate the following questions:

- How does our revised parameterization of surface fluxes (oceanic emissions, soil and leaf uptakes) match with the temporal and spatial variations of atmospheric OCS?
- What is the sensitivity of the phase and amplitude of the simulated seasonal cycles and the sensitivity of the latitudinal gradient of OCS concentrations to changes in surface fluxes?
- Given the current uncertainties on the surface fluxes, how well would optimized fluxes match with the observed time series of atmospheric OCS?
- Can we use the OCS atmospheric observations to benchmark the GPP simulated by current DGVMs, given the uncertainties on OCS surface processes?

In the first section, we describe our new set of tropospheric global sources and sinks of OCS and discuss the spatial and temporal distribution of the fluxes. In a second step, we investigate the resulting OCS atmospheric concentration using a forward modeling

ACPD
14, 27663–27729, 2014

approach. We then analyze the results of the inverse approach in terms of model-data fit and impact on the fluxes. We finally discuss the potential constraint from these results on the GPP of each DGVM.

2 Material and methods

2.1 Global surface fluxes of OCS

2.1.1 Sea-to-air emissions of OCS

OCS is emitted from the oceans to the atmosphere either directly, because surface waters are generally supersaturated in OCS, or indirectly through oxidation of atmospheric dimethylsulfide (DMS) and carbon disulfide (CS_2) which are both produced in the surface layer of the ocean. Oceans are a major source of OCS (Kettle et al., 2002). Berry et al. (2013) found that the marine source accounted for 876 Gg S yr^{-1}, about 74 % of total sources, but this estimate was not well constrained since the authors increased the direct marine emissions of Kettle et al. (2002) by 600 Gg S yr^{-1} to provide a balanced global budget of OCS (Table 1).

Here, the direct emissions are based on parameterizations of ocean production and removal processes of OCS implemented in the NEMO-PISCES oceanic general circulation and biogeochemistry model (Launois et al., 2014). The main production pathway is photochemical, hence light dependent and favored by UV-absorbing chromophoric dissolved organic matter (CDOM). The second pathway, the so-called "dark production", is temperature and organic-matter dependent. The two removal processes are hydrolysis (pH-dependent) and ventilation (dependent on temperature and wind speed). In the standard run defined by Launois et al. (2014), the direct emissions of OCS were equal to 813 Gg S yr^{-1}, with 45 % of emissions coming from the tropical ocean, but other scenarios yielded marine fluxes in the range 573–1763 Gg S yr^{-1}. To represent these high levels of uncertainty on the marine OCS emissions, an allowed variation

ACPD
14, 27663–27729, 2014

range of 70–150 % of the initial simulation of the OCS marine emissions was used in the optimization process (Table 2).

As suggested by Barnes et al. (1994), OCS accounts for 0.7 % of the oxidation products of DMS. Since DMS exhibits a short residence time (Koch et al., 1999; Chin et al., 2000; Kloster et al., 2006), here we assumed that 0.7 % of the marine emissions of DMS were instantaneously converted into OCS. For that, we used a new version of the prognostic module developed by Belviso et al. (2012) to compute seawater DMS concentrations and DMS air–sea fluxes. This module, embedded within NEMO-PISCES as that of OCS, improves the representation of DMS dynamics in subtropical waters (Masotti et al., 2014).

CS_2 emissions from oceans were not computed with NEMO-PISCES but taken from Kettle et al. (2002). We here assumed that 87 % of the marine emissions of CS_2 were instantaneously converted into OCS annually (Barnes et al., 1994).

2.1.2 Uptake of OCS during photosynthesis

Basic principles of the leaf uptake of OCS and CO_2

OCS and CO_2 both diffuse through plant stomata. Since OCS is a heavier and larger molecule than CO_2, it diffuses less rapidly (Berry et al., 2013, and references therein). CO_2 and OCS are both hydrated in leaves by the enzyme carbonic anhydrase (Protoschill-Krebs and Kesselmeier, 1992; Protoschill-Krebs et al., 1995, 1996; Stimler et al., 2010), following:

$$H_2O + CO_2 \leftrightarrow H_2CO_3 \leftrightarrow HCO_3^- + H^+ \quad (1a)$$

$$OCS + H_2O \leftrightarrow HCOOS^- + H^+ \leftrightarrow H_2S + CO_2 \quad (1b)$$

However, $HCOOS^-$ and H_2S are found at very low concentrations in plant cells and soil water (Stimler et al., 2010). Given that H_2S formation is exergonic, thus spontaneous, the hydration of OCS leads irreversibly to H_2S (Schenk et al., 2004). Thus, contrary to

ACPD
14, 27663–27729, 2014

CO_2, irreversible hydrolysis of OCS is expected during photosynthesis (Wöhlfahrt et al., 2012; Simmons et al., 1999; Stimler et al., 2010). When CO_2 produces carbohydrates after carboxylation catalyzed by the enzymes Ribulose-1, 5-bisphosphate carboxylase-oxygenase (Rubisco) or Phosphoenolpyruvate Carboxylase (PEP-Co), H_2S is used for synthesis of amino acids and proteins. Note that OCS is a potential substrate for RuBisCO too, but CO_2 is favored over OCS by a factor 110 for species studied by Lorimer and Pierce (1989). Stimler et al. (2010) noted that no significant cross-inhibition was measured between OCS and CO_2 uptakes.

Selected terrestrial biosphere models

The three DGVMs selected (LPJ, CLM4CN and ORC) had contrasting GPP estimates and various seasonal features. We used the simulated GPP from the TRENDY inter-comparison exercise (see http://dgvm.ceh.ac.uk/), in which all meteorological forcing was standardized. We took the simulated GPP over the 1990–2009 period from the "S2" reference simulations that include the impact of climate change and atmospheric CO_2 increase. In the present paper, we focus on the phase and amplitude of the GPP seasonal cycle from each model, using GPP to compute the uptake of OCS by leaves (as described below).

Parameterization of OCS uptake by plants for each model

In the study by Berry et al. (2013), the OCS leaf uptake was described in a mechanistic way with processes such as diffusion through stomata and the mesophyll, and hydration of OCS molecules, explicitly represented in their vegetation model. Others used a different approach whereby the uptake of OCS was represented in models as a linear function of GPP. We followed the latter approach:

$$F_{OCS} = k_{plant\_uptake} \times (k_{LRU} \times \ GPP), \quad (2)$$

ACPD
14, 27663–27729, 2014

where k_{plant_uptake} is the scaling parameter (set to an initial value of unity, further optimized), and k_{LRU} is the leaf relative uptake of OCS compared to CO_2 (normalized by their ambient concentrations) and defined at the plant functional type level.

As proven by laboratory and field studies, LRU is species-specific and highly variable, especially for C4 plants (Sandoval-Soto et al., 2005; Seibt et al., 2010). Nevertheless, major efforts have been made to estimate the relative deposition rates of OCS and CO_2 (Sandoval-Soto et al., 2005, 2012; Campbell et al., 2008; Seibt et al., 2010; Stimler et al., 2010). Here, we used the results of the study from Seibt et al. (2010) who estimated a global average value for k_{LRU} of 2.8 (± 10 %). This estimate is, however, in the upper range of estimates, since Sandoval-Soto et al. (2005), Stimler et al. (2012) and Berkelhammer et al. (2013) measured values between 1.45 and 3.03 (± 20 to 30 %) for different species. In the Seibt et al. (2010) study, estimated LRUs for the different biomes were in the range 1.55 (xerophytic woods and scrub) to 3.96 (cool/cold deciduous forests). The flux scaling parameter k_{plant_uptake} was allowed to vary in the inverse optimization configuration from 0.7 to 1.3, representing a ±30 % uncertainty range on surface flux initial estimates (Table 2).

A map combining Köppen-Geiger climate zones with phenology-type from satellite land-cover data provided by the MODIS instrument was used to determine the major plant functional type for each region (Poulter et al., 2011; Kottek et al., 2006). Each species was assigned to a Plant Functional Type (PFT) on the previously described map and then assigned the corresponding k_{LRU} relative uptake value from Seibt et al. (2010). The resulting global mask of k_{LRU} was then used to scale the GPP from the three DGVMs to obtain three different global seasonal OCS uptake fluxes by plants.

2.1.3 Soil–atmosphere exchanges

First attempts at investigating air-soil exchanges using soil enclosures and OCS-free air as a flushing gas created an artificial gradient and therefore wrongly suggested that soils were always a large source of OCS to the atmosphere. When atmospheric air is

ACPD
14, 27663–27729, 2014

substituted for flushing soil enclosures, the general picture is that oxic soils are a sink and anoxic soils a source of OCS (Whelan et al., 2013).

OCS uptake by oxic soils

OCS uptake by oxic soils is believed to be essentially a microbial and enzymatically driven process with carbonic anhydrase playing a central role in this soil sink (Chin and Davis, 1993a, b; Seibt et al., 2006; Wingate et al., 2008). There are also clear indications that OCS soil uptake varies according to soil type, temperature and soil water content (Kesselmeier et al., 1999; Van Diest and Kesselmeier, 2008). Kettle et al. (2002) used a temperature and water content-based relationship to estimate the sink of OCS in soils (following the parameterization suggested by Kesselmeier et al., 1999), while Berry et al. (2013) based the OCS uptake by soils on soil heterotrophic respiration (which tracks microbial activity) and soil water content (following the parameterization suggested by Yi et al., 2007).

Here we adopted a different approach to the uptake of OCS by oxic soils, assuming that OCS and di-hydrogen (H_2) deposition to soils share a lot in common. Indeed, H_2 uptake by soils, which represents about 80 % of its total atmospheric loss, is believed to be driven by high H_2-affinity *streptomyces* (Constant et al., 2010). OCS-degrading activity in heterotrophic soil bacteria was associated with isolates belonging to the genera *Mycobacterium* (Kato et al., 2008). *Streptomyces and Mycobacterium* are two important genera of the *Actinobacteria* taxon. Recent studies in genetics and cell biology of *Streptomyces* and *Mycobacterium* have revealed striking similarities in the developmental and morphological hallmarks of their life cycles (Scherr and Nguyen, 2009). Moreover, optimal conditions for OCS (Van Diest and Kesselmeier, 2008) and H_2 soil uptake (Smith-Downey et al., 2006), are rather similar: they both exhibit a broad temperature optimum between 20 and 30 °C (for most soil types) and soil uptake is optimal for low soil moisture (15–25 % of saturation levels). Strong similarities between nighttime deposition velocities of OCS and H_2, in terms of annual mean and ranges of variation, were also inferred from semi-continuous atmospheric observations in a semi-

ACPD
14, 27663–27729, 2014

urban site located 20 km SW of Paris, France. When plotted against H_2 data, the OCS deposition velocities were roughly distributed around the 1 : 1 line (Belviso et al., 2013), but this relationship should perhaps not be applied at the global scale since the deposition velocities recorded in this semi-urban system were in the lower range of deposition velocities recorded by others. However, the airborne measurements carried out by H. Chen above the United States provide support for the existence of such a relationship at the continental scale (H. Chen, personal communication, 2013), but the slope of the relationship was only about 0.5.

Consequently, OCS uptake by soil is therefore represented in our model as:

$$F_{OCS} = k_{soil} \times v_{H_2} \times v_{cos}v_{H_2} \times [OCS]_{atm} \quad (3)$$

where k_{soil} is the scaling parameter controlling the global uptake by soil, v_{H_2} the deposition velocity into the soil and $v_{cos}v_{H_2}$ the relative ratio of OCS and H_2 deposition velocities.

Two different approaches to estimating v_{H_2} are used here. The first one is that of Morfopoulos et al. (2012) who implemented a hydrogen uptake module in the LPJ-WHyME model, including a description of atmospheric H_2 diffusion through soil (Fick's first law) and of the biological processes of uptake which are limited by soil temperature and soil water content. The second approach is that of Bousquet et al. (2011) who used an atmospheric inversion model of global and regional fluxes, based on a global network of flask observations of H_2 concentration.

Given the uncertainties associated with the v_{H_2} estimates and the ratio between OCS and H_2 deposition velocities, $v_{cos}v_{H_2}$ was set to an initial value of 0.75 (in the standard run) and the surface fluxes were further optimized with a 30 % range of variation allowed for the k_{soil} scaling coefficient (Table 3).

Release of OCS from anoxic soil

The role of soils in the OCS budget was recently reviewed by Whelan et al. (2013), with special attention being paid to anoxic soils. The authors underlined the major

ACPD
14, 27663–27729, 2014

influence of soil temperature and flooding on OCS emissions from anoxic soils and wetlands. Therefore, the way the OCS emissions by anoxic soils were represented in our model was largely based on the Whelan et al. (2013) inventory. However, because large uncertainties were associated with those fluxes (see Fig. 3 in Whelan et al. (2013), "soil only" case), we finally assigned zero emission of OCS to rice paddies and 25 pmol m^{-2} s^{-1} to peatlands. We used the seasonal maps by Wania et al. (2010) of emission of methane from both categories of soils, as simulated using the LPJ-WHy-ME model, to locate both in time and space the hot spots of OCS emissions from anoxic soils. Unfortunately, salt marshes, which are strong emission sites of OCS (Whelan et al., 2013), are not taken into account in the LPJ-WHy-ME model.

For optimization purpose, those modeled fluxes were also assigned a k_{anoxic_soil} scaling factor. Given the uncertainties over this parameterization, k_{anoxic_soil} was optimized with an assigned a ±30 % variation range allowed to rescale the OCS emissions from anoxic soils (Table 3).

2.1.4 Other sources and sinks

Other sources are related to biomass burning, and direct and indirect anthropogenic emissions. OCS emissions from biomass burning were simulated from the gridded CO_2 emission maps of Van der Werf et al. (2010) (GFEDv3 product) rescaled to a source of 70 Gg S yr^{-1}, as estimated by Nguyen et al. (1995). The uncertainty associated with these emissions in the optimization procedure was set to ±10 % (maximum range of variation). Both direct and indirect anthropogenic emissions were taken from the global gridded fluxes proposed by Kettle et al. (2002). These fluxes were attributed a ±10 % maximum variation in the optimization scheme. Additional direct and indirect emissions of OCS by volcanoes were neglected because they are highly uncertain (Belviso et al., 1986).

The removal of atmospheric OCS by OH radicals is also a significant sink of OCS. We used monthly maps of OH radicals provided by Hauglustaine et al. (1998) that we integrated vertically up to the tropopause, to distribute both horizontally and temporally

ACPD
14, 27663–27729, 2014

a total annual atmospheric sink of 100 Gg S yr^{-1}, as suggested in previous global budgets. This flux was attributed a ±30 % maximum variation when using the optimization scheme.

2.2 Atmospheric transport model

The simulated mixing ratios were obtained using the Global atmospheric Circulation Model (GCM) of the Laboratoire de Météorologie Dynamique (LMDz, version 3; Hourdin et al., 2006). The OCS surface fluxes described above are transported in an offline mode using the LMDz transport model, nudged with wind from the European Centre for Medium-Range Weather Forecasts (ECMWF) reanalysis. The transport model uses a 3.75° × 2.5° (longitude × latitude) horizontal resolution and 19 vertical layers between the surface and the top of the troposphere. LMDz has been previously used in many tracer transport studies (Chevallier et al., 2010; Carouge et al., 2010a, b). In this study we used a pre-calculated transport field, corresponding to the sensitivity of the monthly concentration at each site with respect to the daily surface fluxes for all pixels of the transport grid (see Peylin et al., 2005). These pre-calculated sensitivities were derived from the adjoint of the transport model and were multiplied by the surface fluxes to get the atmospheric OCS concentration. They will also be directly used in the inversion (see below) as the optimization algorithm requires the sensitivity of the concentrations to the surface fluxes.

2.3 OCS atmospheric observations

Atmospheric OCS and CO_2 concentrations used in the present work are from the NOAA/ESRL (**N**ational **O**ceanic and **A**tmospheric **A**dministration/**E**arth **S**ystem **R**esearch **L**aboratory/Global Monitoring Division Flask Program) database, where OCS measurements from 10 stations have been gathered since 2000 (Montzka et al., 2004). These stations include 9 background sites (SPO, South Pole; CGO, Cape Grim, Tasmania, Australia; SMO, American Samoa; MLO, Mauna Loa, Hawaii, United States;

ACPD
14, 27663–27729, 2014

NWR, Niwot Ridge, Colorado, United States; BRW, Barrow, Alaska, United States; ALT, Alert, Nunavut, Canada; MHD, Mace Head, Ireland; KUM, Cape Kumukahi, Hawaii, USA) and a single continental site (LEF, Wisconsin, United States). The location of stations is shown in Fig. 1.

Samples were analyzed using gas chromatography and mass spectrometry. Precision is better than 6.3 ppt (14 ppt for SPO). OCS data are available for the scientific community at ftp://ftp.cmdl.noaa.gov/data/hats/carbonylsulfide. The typical measurement error for OCS is 6.3 ppt, much lower than the transport model error. Note that CO_2 data used in this study were downloaded from (ftp://ftp.cmdl.noaa.gov/ccg/co2/). For CO_2, we assumed a typical 0.1 ppm measurement error on the observations. More details of the OCS and CO_2 measurement techniques are given by Montzka et al. (2004).

2.4 Optimization framework

2.4.1 Principle

We used an optimization algorithm to correct the surface OCS fluxes in order to improve the simulation of atmospheric OCS temporal and spatial gradients. The optimization scheme relies on a Bayesian framework approach that accounts for prior knowledge of the surface fluxes (Tarantola, 1987). The optimized variables correspond to global scalars applied to all OCS surface flux components described above. Each flux has been assigned a scalar coefficient x to account for uncertainties in the calculation of the OCS fluxes; their optimization will provide a better agreement between modeled and observed atmospheric OCS concentrations. The allowed range of variation on the x coefficient was determined for each surface flux after analysis of the uncertainties (see Sect. 2.1).

ACPD
14, 27663–27729, 2014

2.4.2 Cost function and gradient-based algorithm

Assuming a Gaussian probability density function (PDF) distribution for the measurement errors, the model structure errors (including flux and transport models) and the model parameter errors (flux scalars), the optimal set of parameters under the Bayesian framework corresponds to the minimum of the following cost function $\mathbf{J}(x)$ (Tarantola, 1987):

$$\mathbf{J}(x) = (\boldsymbol{Y} - \boldsymbol{M}(x))^T \mathbf{R}^{-1} (\boldsymbol{Y} - \boldsymbol{M}(x)) + (\boldsymbol{x} - \boldsymbol{x}_\mathrm{p})^T \mathbf{B}^{-1} (\boldsymbol{x} - \boldsymbol{x}_\mathrm{p}) \quad (4)$$

Where $\boldsymbol{x}$ are the parameters to be optimized (i. e., the OCS surface flux scalars), $\boldsymbol{x}_\mathrm{p}$ their a priori values, $\boldsymbol{Y}$ the vector of observations (i.e., the measured OCS mixing ratios at NOAA sites), $\boldsymbol{M}(x)$ the model outputs (i.e., the OCS mixing ratios simulated with the LMDz transport model). **R** and **B** are error covariance matrices, which describe the prior variances/covariances of observations and parameters, respectively. The **R** matrix includes the analytical errors, the transport model errors and the representation errors in the transport model (the scale mismatch between measured and simulated concentrations). Correlations in **R** are too difficult to assess and therefore neglected. Uncertainties on the a priori flux scalar values (**B** matrix) are set to large values (see below) which minimizes the influence of this term in the cost function. Moreover, error correlations between a priori parameter values were also neglected.

The first term of $\mathbf{J}(x)$ represents the weighted data-model squared deviations (i.e. the misfit between the simulated outputs and the corresponding observational data), while the second term represents the mismatch between optimized and prior values, weighted by the prior uncertainties on parameters.

Given that we optimize scalars of the OCS surface fluxes and that the OCS destruction by OH in the atmosphere is fixed (i. e., prescribed and independent of the atmospheric OCS concentrations), the optimization problem is linear (i. e., the atmospheric concentrations linearly depend on the surface fluxes and their scaling factors). $\boldsymbol{M}(x)$ is thus equal to $\boldsymbol{M}.x$, with $\boldsymbol{M}$ now representing the pre-calculated model concentration sensitivities to surface fluxes. With this assumption, the minimum of the cost

ACPD
14, 27663–27729, 2014

function can be obtained directly with a matrix formulation of the inverse problem (see for instance Tarantola, 1987). Note that in order to account for bounds on each flux parameter, we iterated the scheme seven times. At each of the iterations, the optimized value for each parameter may be outside its range of variation. In this case, we fixed the parameter value (flux scalar) to its boundary and re-optimized excluding the parameter from the optimization. We then repeated the process until all parameters were fixed or within their range of variations.

Finally, assuming Gaussian errors, the posterior error covariance matrix on the parameter can be directly estimated from a matrix formulation.

2.4.3 Optimization setup and optimized parameters

The optimization scheme is based on a 5 year-long simulation covering the 2004–2009 period, long enough to characterize most broad atmospheric OCS features (trends and mean seasonal cycles). The observed OCS raw data are used for the optimization. We thus selected for each data point the closest monthly mean simulated concentration to compare with (outputs from the LMDz transport model were only saved on a monthly time-step). The optimized fluxes correspond to all sources and sinks of Table 2, to which the scaling coefficients are applied for each corresponding flux component.

For each parameter, we assigned a possible range of variation as well as a prior error (1-σ SD). In the standard configuration, prior parameter values equal to 1.00 and their prior uncertainty was set to 30 % while the range of variation was set to ±30 %, except for the direct oceanic emissions (range and uncertainty of −30/+50 %), the OCS emitted through biomass burning and anthropogenic activities (range of ±10 % and uncertainty of 10 %). These relatively large errors, combined with the range of variations defined above for each flux component, account for current uncertainties on the OCS processes that control the different sources and sinks. We also performed sensitivity tests on the optimization (Table 3), using a limited 10 % error and restricted ranges of variation for all scaling factors (±10 %), referred as the Low-Error optimization scenario ("OPTIM_L-Er"). This test assumes that our OCS flux models (leaf and soil

ACPD
14, 27663–27729, 2014

uptake, ocean release, etc.) are accurate which would thus reveal the potential biases in the simulated atmospheric OCS levels (phase, amplitude, trend) due to other drivers of the OCS signal, such as GPP fluxes and transport model errors. The main objective is indeed to reveal any remaining biases (after the optimization), which could suggest corrections to the GPP fluxes, underlying the OCS leaf uptake model.

The different stations are assigned different weights in the optimization algorithm, represented as observation monthly errors, depending on the uncertainties associated with the LMDz model for each station. The uncertainties combine the analytical errors, the forward model errors in the transport model and the representation errors in the transport model (the mismatching scales of the measurements and the transport model). Since the impact of plant and soil uptakes are larger in the Northern Hemisphere and therefore the atmospheric levels of OCS show larger amplitude in their seasonal variations, observation errors are set to a higher range in Northern Hemisphere stations (set to 26 ppt), while stations from tropical regions are assigned 20 ppt error and extra-tropical stations from the Southern Hemisphere are assigned 13 ppt error (these regions being mostly influenced by oceanic fluxes). These errors represent about 5 % of the signal (i.e., OCS mixing ratios).

2.5 Experiments and data processing

2.5.1 Forward simulations for OCS

A series of simulations was performed, for which initial conditions are summarized in Table 3. We carried out three runs using the three different DGVMs ("STD_ORC", "STD_LPJ", "STD_CLM4CN"), four sensitivity experiments to the representation of soil uptake in the ORC model ("TEST_SOIL_MORF_1:1", "TEST_SOIL_MORF_0.5:1", "TEST_SOIL_BOUSQ_1:1", "TEST_SOIL_BOUSQ_0.5:1"), and two sensitivity experiments to changes in magnitude of oceanic emissions ("TEST_OCE_+30" and "TEST_OCE_−30") using the ORC model too. Note that the other surface fluxes were kept unchanged in the simulations and sensitivity tests (OCS oxidation by OH radicals,

ACPD
14, 27663–27729, 2014

emissions from anoxic soils and wetlands, direct and indirect anthropogenic emissions, and emissions from biomass burning).

2.5.2 Forward simulations for CO_2

An additional series of simulations was performed to compute the CO_2 concentrations at the same stations as those used for OCS. The LMDz transport model was forced with the net ecosystem carbon fluxes from the three vegetation models (ORC, LPJ, CLM4CN), also using air–sea exchange from the climatology of Takahashi et al. (2008), the biomass burning fluxes from GFEDv3. 1 (Van der Werf et al., 2010) and fossil fuel emissions from EDGARD-v4. 1 (Marland et al., 1999). Simulations with only the gross ecosystem carbon fluxes contributions (GPP and respiration) were also performed separately, showing the individual impact of both gross fluxes on the CO_2 seasonal cycle at all stations.

2.5.3 Optimization scenarios for OCS

We also conducted three series of optimization experiments of surface fluxes, each carried out with a different vegetation model (Table 3). We tested systematically five different scenarios:

- "OPTIM_H-Er", where the marine, soil and vegetation fluxes are allowed to vary over a large range,
- "OPTIM_L-Er", where the marine, soil and vegetation fluxes are allowed to vary over a narrow range,
- "OPTIM_Leaf_ONLY", where only leaf fluxes are allowed to vary over a large range,
- "OPTIM_Soil_ONLY", where only soil fluxes are allowed to vary over a large range,

ACPD
14, 27663–27729, 2014

– "OPTIM_Ocean_ONLY", where only ocean fluxes are allowed to vary over a large range.

See Table 3 for details. All other fluxes (OCS oxidation by OH radicals, emissions from anoxic soils and wetlands, direct and indirect anthropogenic emissions, and emissions from biomass burning) were kept unchanged.

2.5.4 Data processing and analysis

OCS and CO_2 raw data from models and observations were processed to derive mean seasonal cycles and mean annual trends. For that, raw data were fitted with a function including a polynomial term (1st order) and four harmonics. The residuals of the functions were further smoothed in the Fourier space, using a low pass filter (cutoff frequency of 65 days) to define a so-called smoothed curve (function plus filtered residuals). The mean seasonal cycle is defined from the smoothed curve after subtraction of the polynomial term.

To allow for a precise analysis of the mismatches between simulated and observed OCS concentrations, the mean square error (MSE) was decomposed into three components (bias, phase and variance), as described by Kobayashi and Salam (2000), following:

$$\mathrm{MSE} = (\langle X_i \rangle - \langle X_{i'} \rangle)^2 + (\sigma_i - \sigma_{i'})^2 + 2(\sigma_i \times \sigma_{i'})(1 - r)^2 \quad (5)$$

where the meaning of the squared data bias is obvious, the second term indicates differences in the fast variability, and the lack of correlation r between X_i and $X_{i'}$ is a very simple estimator for phase errors.

ACPD
14, 27663–27729, 2014

3 Results

3.1 Surface fluxes

Figure 1 examines the spatial variations in the intensity of mean emissions and uptakes of OCS by the oceans and the terrestrial biosphere (soils and vegetation) for the months of January and July, as calculated from the new parameterizations presented above. The corresponding annual fluxes, spatially averaged over oceans and continents, can be found in Table 1.

3.1.1 Oceanic fluxes

Direct emissions

Following the standard run defined by Launois et al. (2014), oceans emit a total of 813 Gg S each year (Table 1). The seasonality of fluxes in the mid and high latitudes of both hemispheres is essentially controlled by sea surface OCS photoproduction and hydrolysis. Winter fluxes are slightly negative (oceans take up OCS from the atmosphere, Fig. 1, top), whereas summer fluxes are largely positive (they range between 3 and 10 pmol m^2 s^{-1}). In the tropical regions (30° S–30° N), the annual total fluxes are important (45 % of OCS emissions) and rather invariant (6 to 8 pmol m^2 s^{-1}). In this case, the major controlling factors are light and sea-surface temperature (SST) through SST-mediated dark production of OCS (Launois et al., 2014). Note the presence of an OCS emission "hot spot" off the coast of Somalia in July (up to 25 pmol m^2 s^{-1}), a feature linked to intense upwelling simulated by the NEMO-PISCES model on which our marine emission maps rely. Overall, our simulations show direct oceanic emissions to be about 20 times larger than those from Kettle et al. (2002) and are roughly comparable to the estimates Berry et al. (2013) obtained by inverse optimization (Table 1).

ACPD
14, 27663–27729, 2014

Indirect emissions

On a yearly and global basis, the oceans are also a net source of DMS and CS_2 to the atmosphere. In NEMO-PISCES, each year 133 Gg S are indirectly injected into the atmosphere from DMS, assuming that 0.7 % of the total emissions are converted into OCS. This estimate and that of Kettle et al. (2002) are in good agreement. Global maps of OCS emissions from DMS atmospheric oxidation for the months of January and July are provided in the Supplement (Fig. A1). Most of the OCS indirect emissions occur at high latitudes in the Southern Hemisphere, regions where the amplitude of the seasonal cycle is also the most important, with seasonal emissions varying between 4 and 7 Gg S per month (Fig. A1 in Supplement).

Ocean fluxes of CS_2 rely on those of Kettle et al. (2002), since they are not parameterized in NEMO-PISCES. Globally, CS_2 indirectly brings 81 Gg S yr^{-1} of OCS into the atmosphere, as 87 % of the CS_2 is assumed to be oxidized into OCS. CS_2 fluxes are mostly emitted in tropical regions, but again present a larger seasonal amplitude in the extra-tropical regions than in the tropics.

3.1.2 Soil fluxes

As described in Sect. 2.1.3, oxic soils are a sink and anoxic soils a source of OCS. Global maps of OCS exchange between soil and the atmosphere are shown in Fig. 1 (middle row) for the months of January and July.

Oxic soil uptake of OCS

Using the H_2 deposition velocities by Morfopoulos et al. (2012) and 0.75 as the ratio between the deposition velocities of OCS and H_2 (our standard case), the resulting simulated uptake of OCS by oxic soils ranges between 0 and 15 pmol m^2 s^{-1} (Fig. 1) and account for a global annual uptake of 510 Gg S (Table 1). This uptake is about three times larger than the soil uptake modeled by Kettle et al. (2002) and

ACPD
14, 27663–27729, 2014

40 % larger than the one reported by Berry et al. (2013). The sensitivity of monthly uptake rates to the choice of contrasted uptake scenario is evaluated in Fig. A2 (in Supplement), at the global scale and by large bands of latitude. The largest total uptake of OCS by oxic soils is obtained using the "TEST_SOIL_MORF_1:1" scenario (700 Gg S yr^{-1}, with a ratio of OCS to H_2 deposition velocity of unity. In this case, the extra-tropical areas of the Northern and Southern Hemispheres each account for 30 % of total uptake, and the remaining is taken up by tropical regions. The smallest total uptake of OCS by oxic soils is obtained using the "TEST_SOIL_BOUSQ_0.5:1" scenario (330 Gg S yr^{-1}). In this latter case, the extra-tropical areas of the Northern and Southern Hemispheres, and the tropical regions account for 53, 29 and 18 % of the total uptake, respectively. Whatever the magnitude of the ratio between deposition velocities, the seasonal variations are more important in the extra-tropical areas of the Northern Hemisphere than elsewhere, and they differ between models of H_2 deposition rates ("TEST_SOIL_BOUSQ" versus "TEST_SOIL_MORF"). Indeed, in "TEST_SOIL_BOUSQ" the OCS sink reaches a peak in spring whereas maximum uptake rates are seen in summer in "TEST_SOIL_MORF".

Anoxic soil fluxes

The emissions from anoxic soils, parameterized as described in Sect. 2.5, mainly take place in the northernmost regions (above 60° N), where fluxes up to 12.5 pmol m^2 s^{-1} were simulated (Fig. 1). Total emissions are estimated to be 101 Gg S on an annual basis (Table 2). OCS emissions by peatlands can turn the extra-tropical regions of the Northern Hemisphere into a net source of OCS in late autumn and winter.

Net soil fluxes

Overall, at a global scale, soils constitute a net sink of OCS. In the Northern Hemisphere our estimated sink is lower than that of Kettle et al. (2002) and that of Berry et al. (2013) where the OCS emissions by anoxic soils were not taken into con-

ACPD
14, 27663–27729, 2014

sideration. Using the "TEST_SOIL_BOUSQ_1:1" configuration, the simulated fluxes vary between +1 and −15 Gg S per month in the Northern Hemisphere (Fig. A2), while they range between +3 and −8 Gg S per month using "TEST_SOIL_MORF_1:1". In the tropics, the simulated fluxes also display large variations (between −2 and −8 Gg S with "TEST_SOIL_MORF_1:1", between −11 and −14 Gg S per month with "TEST_SOIL_BOUSQ_1:1"). The same configurations lead to variations respectively between −3 and −12 Gg S per month and between −7 and −11 Gg S per month in the Southern Hemisphere.

At the global scale, the monthly fluxes of OCS vary between 0 and −28 Gg S per month (using Bousquet et al., 2011) and between −15 and −28 Gg S per month (using Morfopoulos et al., 2012). These large soil flux seasonal variations will significantly impact the simulated OCS atmospheric seasonal variations. We also notice that for all configurations, the largest amplitude of the OCS flux variations are found in the Northern Hemisphere.

3.1.3 Plant uptake

Global maps of OCS mean uptake by plants for the months of January and July, constructed from the GPP of the ORC model, are shown in Fig. 1 (bottom). On an annual basis, plants take up 1335 Gg S (Table 1), which is a considerably larger sink than that modeled by Kettle et al. (2002) or Berry et al. (2013). Note that this number is strongly model-dependent as shown in Table 1 and Fig. A3 (in Supplement). The differences between the three models of GPP in terms of phase and amplitude of the seasonal variations are shown in Fig. A3 (in Supplement), displayed as large latitudinal bands in the Northern Hemisphere. Because OCS uptake by plants is represented in our models as a linear function of GPP (Eq. 2), the phase and amplitude of the seasonal variations in OCS plant uptake and GPP have the same patterns.

The ORC model displays stronger OCS uptake than the other models, throughout the year and especially during the summer months (Fig. A3 in Supplement). In ORC, the extra-tropical regions of the Northern Hemisphere are responsible for this summer up-

ACPD
14, 27663–27729, 2014

take and account for about a third of the total plant uptake. The uptake of OCS in tropical regions is roughly constant and accounts for 45 % of the total uptake. The remaining 20 % is contributed by the extra-tropical regions of the Southern Hemisphere where the intensity of the summer maximum (about 35 Gg S month^{-1}) is roughly a quarter of that occurring in the Northern Hemisphere. Figure A3 (in Supplement) reveals large differences in the amplitude of seasonal variations depending on which biospheric model is used to model the leaf uptake (the respective seasonal amplitudes are between 50 and 95 Gg S per month for ORC and CLM4CN). Large differences in the modeled OCS level seasonal phase can also be seen. Indeed, plant uptake reaches a peak in late spring in CLM4CN while maximum uptake occurs later in the year in the other models (the time lag is about two months).

3.1.4 Other sources and sinks, and global budgets

An OCS sink of about 100 Gg S yr^{-1}, representing its photochemical oxidation by OH radicals, was implemented as described in the methods section. The resulting total annual uptake is relatively evenly distributed as a function of latitude but shows larger seasonal variations at high latitudes than in the tropics (data not shown).

The direct and indirect anthropogenic fluxes were those assessed by Kettle et al. (2002), who estimated that 180 Gg S are emitted on an annual basis, without strong seasonal variations. The anthropogenic fluxes of OCS are almost entirely emitted in eastern Asia, eastern Europe and the eastern part of both Canada and the United States of America.

As described in the methods section, the OCS emissions from biomass burning were arbitrarily scaled (from CO_2 emissions) to reach a total of 70 Gg S yr^{-1}, to match the estimates of Nguyen et al. (1995). Tropical regions account for about 60 % of total emissions, and tropical emissions are quite evenly distributed throughout the year. Elsewhere, the emissions vary seasonally, reaching their maximum in summer, and, on an annual basis, are smaller in the Southern than in the Northern Hemisphere.

ACPD
14, 27663–27729, 2014

Table 1 provides an overview of the magnitude of the sources and the sinks in the global budget of OCS, and of the total net flux. Global budgets are also compared between them. Only Kettle et al. (2002) and Berry et al. (2013) have provided balanced budgets between sources and sinks, but it is worth remembering here that Berry et al. (2013) increased the marine emissions of Kettle et al. (2002) by 600 Gg S yr^{-1} for this purpose. Other budgets including ours are largely unbalanced, with sinks exceeding sources by hundreds of Gg S yr^{-1}. The budget of Montzka et al. (2007) and the one we raised using ORC's GPPs are the most unbalanced (−776 and −566 Gg S yr^{-1}, respectively).

3.2 Forward modeling of atmospheric OCS concentrations

To assess our current understanding of the biogeochemical cycle of OCS and its dynamics in the atmosphere, we transported surface fluxes with LMDz in a forward approach. Global monthly 3-D fields of atmospheric OCS mixing ratios were generated and then compared with in situ observations gathered by the NOAA atmospheric network. Special attention has been paid to the annual, seasonal and latitudinal variations of this gas.

3.2.1 Annual trends

Mauna Loa (MLO) is a mid-latitudinal background station in the middle of the tropical Pacific Ocean (20° N, altitude 3500 m). The data therefore represent the integrated the contribution of the surface fluxes from the entire Northern Hemisphere (Conway et al., 1994). Figure 2 compares the simulated monthly mean atmospheric OCS concentrations (using the "STD_ORC" configuration for surface fluxes, Table 3) with the observations at MLO and with other simulations (Kettle et al. (2002), "STD_LPJ", and "STD_CLM4CN" configurations of surface fluxes, Table 3).

Our three standard simulations are based on strongly unbalanced budgets (Table 1). Consequently, those simulations show negative annual trends (23 to 70 ppt yr^{-1}), a pat-

ACPD
14, 27663–27729, 2014

tern inconsistent with observations. Since Kettle et al. (2002) proposed a roughly balanced OCS budget (the difference between sources and sinks is in fact slightly positive), the OCS atmospheric levels show a small positive annual trend. However, the amplitude of the seasonal variations using Kettle et al. (2002) is too small when compared with the observations.

The situation at the South Pole (SPO) resembles that at MLO in terms of annual trends (Fig. 3). This is again a consequence of the use of unbalanced budgets. We also explored the impact of oceanic emissions of OCS on the annual trend at MLO and SPO using sensitivity tests where the marine fluxes were increased or decreased by 30 % (TEST_OCE_+30 and TEST_OCE_−30, resp.; Fig. 3). The importance of the oceanic emissions of OCS in the global budget is confirmed since a 30 % increase in oceanic fluxes markedly reduces the negative annual trend at both stations.

As described above, the uptake of OCS by oxic soils is proportional to the deposition velocity of H_2 and to the ratio between OCS and H_2 deposition velocities (assumed to be equal to 0.75 in the standard run named "STD_ORC", Table 3). The impact of the oxic soils on the annual trend is explored at MLO via a series of four sensitivity tests (Fig. 4, left panel). Results show that the annual trend is more affected by changes in v_{OCS}/v_{H_2} ratios than by changes in the way H_2 deposition velocities have been estimated. Indeed, the difference in annual trend is smaller than 10 ppt yr^{-1} between the "TEST_SOIL_MORF" and "TEST_SOIL_BOUQ" simulations, whereas it is about 25 ppt yr^{-1} between the respective "1:1" and "0.5:1" simulations. Note that neither changes in the marine emissions nor changes in OCS uptake by oxic soils can individually compensate for the strong negative trend imposed by the vegetation sink of the ORC model.

3.2.2 Phase and amplitude of seasonal variations

Detrended and smoothed curves are used to investigate the differences in terms of phase and amplitude of seasonal variations between a series of simulations at the

ACPD
14, 27663–27729, 2014

position of the SPO, MLO and Alert (ALT) stations. The ALT data help in exploring the influence of boreal and temperate ecosystems of the Northern Hemisphere on the biogeochemical cycle of OCS. Figure 5 (right panels) compares the seasonality of OCS air concentrations between four different simulations and the observations, while data shown in the right panel of Figs. 3 and 4 aim at characterizing the sensitivity of seasonal variations to changes solely in marine emissions and in the soil sink, respectively.

The ORC model (but to a lesser extent LPJ too) displays the highest seasonal amplitudes both at ALT and MLO (about 250 and 80 ppt, respectively) which are unrealistically high as compared with observations (100 and 55 ppt respectively, Fig. 5). However, ORC is more in phase with observations than the other simulations, especially at ALT. The simulation based on the Kettle et al. (2002) data exhibits amplitudes which are unrealistically low and not in phase with the observations at ALT and MLO. At ALT, CLM4CN simulates the right amplitudes but represents the phase incorrectly. This model provides a better representation of the phase of the OCS cycle at MLO but leads to a 10 % underestimation of the OCS seasonal amplitude. At SPO, on the contrary, the simulation based on the Kettle et al. (2002) data and the observations fit very well both in terms of seasonal amplitude and of phase. Other models simulate slightly larger amplitudes (+10–15 ppt relative to observations) and a slight shift in the OCS maximum in austral summer.

At MLO, the phase and the amplitude of the seasonal variations are apparently unaffected by changes in marine emissions (Fig. 3) and changes in oxic soils uptake (Fig. 4). At SPO, the amplitude of the seasonal variations is clearly modulated by changes in marine emissions of OCS (Fig. 3): a 30 % increase of the ocean flux leads to about a 10 % increase in amplitude of the seasonal variations.

A last experiment specifically addressed the constraints that air-plant exchanges put on the seasonality of OCS. This was done by comparing our standard runs (STD_ORC, STD_LPJ and STD_CLM4CN) with runs where only the uptake of OCS by plants was transported by the LMDz model. Figure 6 shows that the amplitude and the phase of the seasonal variations at ALT and MLO are both determined by the loss of OCS to

ACPD
14, 27663–27729, 2014

vegetation, the other components having a much lower contribution and canceling out (not shown). On the other hand, plants can have no control at all on the seasonality at SPO, where there is no vegetation.

3.2.3 Annual mean concentrations of OCS: north–south gradients

Annual mean mixing ratios for the 10 stations of the NOAA monitoring network, plotted as a function of latitude, are shown in Fig. 7. Note that the simulated global mean OCS concentration (across all sites) has been rescaled to the observed global mean, so that only the gradients between stations should be investigated. The main results from this diagnosis are:

- Our new OCS surface flux scenarios capture the main differences in annual mean concentration between stations with lower concentrations at continental stations in the Northern Hemisphere (LEF, BRW, ALT) than at background stations as in the Southern Hemisphere (around 50 ppt lower).
- Observed differences between southern extra-tropical marine stations and tropical marine stations (higher concentration over the tropics by 10 ppt) are also represented by the different scenarios.
- Significant discrepancies still affect all scenarios, such as for instance, the difference between NWR and LEF, with simulated values around 25 to 30 ppt compared to observed ones around 60 ppt.
- There are small but significant differences between the three scenarios based on three different ecosystem models. For instance, between Cape Grim (CGO) and American Samoa (SMO), although all models largely overestimate the mean concentration gradient, using CLM4CN reduces it by nearly 20 ppt compared to ORC. The difference between SPO and CGO is also much larger in ORC than in LPJ or CLM4CN, while the observations show no differences. Similarly, CLM4CN gives a lower annual mean concentration at Point Barrow (BRW) than at Alert

ACPD
14, 27663–27729, 2014

(ALT) while the two others models give higher concentrations at BRW, in line with the observations.

– Note that the simulation based on the Kettle et al. (2002) fluxes shows much smaller annual mean gradients across stations than our three scenarios, whereas the OCS network recorded lower levels of OCS in the extra-tropical Northern Hemisphere (LEF, BRW and ALT exhibit mean levels lower than 460 ppt). This first OCS global budget especially misses the larger tropical mixing ratios (25° S–25° N). The better match between the observed gradients and our new flux scenarios partly arises thanks to the re-estimated high oceanic emissions in the tropical regions.

Two sensitivity tests have been conducted, where ocean emission and soil uptake were increased by 30 % (TEST_OCEAN_+30 and TEST_SOIL_MORF_1:1, respectively). We note that soil or ocean flux modifications have little influence on the resulting atmospheric mixing ratios when compared with the "STD_ORC" run (Fig. 7, dotted and dashed lines). They only affect significantly the gradients in the southern extra-tropical region (7 ppt change in the gradient between CGO and SPO, between the "STD_ORC" and the "TEST_SOIL_MORF_1:1" simulations).

3.3 Optimization of surface OCS fluxes

Here we present the result of the optimizations, described in the methods Sect. 2.5. The principle is to scale each surface flux component in order to obtain the best fit to the atmospheric OCS concentrations (raw data). The main objective is to investigate whether the optimization of the three scenarios, based on the three ecosystem models, can match the observed temporal and spatial OCS variations and can highlight corrections on the GPP that would be needed to improve the representation of the OCS atmospheric levels.

Table 2 summarizes the initial and the optimized values of the surface fluxes, for the different optimization configurations. Note that in the standard cases ("OPTIM_H-Er"

ACPD
14, 27663–27729, 2014

configuration), a large range of variations (i.e., ±30 % changes in individual surface fluxes), along with large prior error (see Table 3).

3.3.1 Optimization of the annual trends

The OCS monthly mean concentrations (raw data) simulated with the optimized surface fluxes (using "OPTIM_H-Er" scenarios) are shown in Fig. 8. The simulated annual trends (displayed over three years only) have been significantly reduced (compare Figs. 8 and 2). Hence, the allowed range of variation for the surface fluxes is sufficiently large to yield equilibrated global budgets after optimization, as suggested by the observations (see the last line of Table 2). This is especially true for ORC ($-566\,\mathrm{Gg\,S\,yr^{-1}}$ before optimization, $-6\,\mathrm{Gg\,S\,yr^{-1}}$ after optimization). When the allowed range of variation for all flux scalars and their prior uncertainty are reduced (i.e., low error case, "OPTIM_L-Er"), a negative trend of about $30\,\mathrm{ppt\,yr^{-1}}$ remains with ORC (Fig. 8). This "OPTIM_L-Er" configuration could be thought as a case where the values of k_{LRU} (for OCS leaf uptake) would be well constrained as well as the fluxes controlled by soil, ocean and anthropogenic processes. In this theoretical case, the mismatch between the simulated and observed annual trend for ORC would suggest: (i) the determinant role played by the vegetation sink in the OCS global atmospheric budget, and (ii) that the leaf uptake of OCS is too large when using ORC, highlighting a too large global annual GPP flux.

3.3.2 Optimization of the amplitude of the seasonal variations

Figure 9 shows the OCS mean seasonal cycles at the stations of the NOAA-ESRL network, before and after optimization, using the three DGVMs. At most stations, the optimization of the surface fluxes significantly reduces the differences in seasonal amplitude between simulations and observations. The global RMSE for the three different DGVMs, computed from the monthly mean seasonal cycle, was reduced from 162 (resp. 83) to 29 (resp. 29) ppt for ORC (resp. LPJ) and from 43 to 35 ppt for CLM4CN.

ACPD
14, 27663–27729, 2014

Although all optimizations lead to a significant improvement of the amplitude of the OCS cycle, differences between the three models are highlighted:

- With the ORC model, the standard optimization ("OPTIM_H-Er" configuration) strongly reduces the amplitude of the simulated OCS seasonal cycle at all stations of the Northern Hemisphere and especially at high latitudes (e.g., at ALT it decreases from 225 to 140 ppt). The optimized amplitudes are more consistent with the observed ones but are still slightly too large at high latitudes (140 versus 100 ppt at ALT). At MLO, the amplitude of the OCS levels is reduced from 80 to 45 ppt, a value slightly lower than the observations (50 ppt). We note that scaling the surface fluxes through the optimization leads to negligible modifications of the phase of the simulated OCS concentrations.
- With the LPJ model, the optimization of the surface fluxes leads to an equal reduction of the sinks and sources, which translates into a reduction of the simulated amplitude of the OCS annual cycle. The optimized fluxes lead to the best representation of the amplitude of the OCS annual cycle at temperate latitudes compared with the observations. However, the optimization does not improve the phase of the atmospheric OCS signal with, therefore, the same caveat at northern stations as for the prior, i. e., a phase shift of nearly two months at ALT and BRW (earlier maximum and minimum).
- With CLM4CN configuration, the optimization does not significantly improve the mean seasonal cycle, with prior and posterior amplitudes that are too small at high northern sites compared to the observations (reaching 60 and 75 % of the yearly amplitude observed at ALT and MLO, respectively). The phase is also not changed and most discrepancies noticed above (Sect. 3.2.2) remain: advance of the maximum and minimum was even larger than for LPJ (more than two months at BRW).

Overall, the above improvements are met with significant changes in the fluxes: the total sink is decreased in all optimization results, whichever GPP is used to model

ACPD
14, 27663–27729, 2014

the leaf uptake of OCS. The average value (between models) has been reduced from 1721 Gg S yr^{-1} in the prior simulation to 1280 Gg S yr^{-1} after optimization, which represents a reduction of 26 %. The source flux estimates were also reduced by 8 % on average, from 1379 Gg S yr^{-1} in the prior simulation to 1270 Gg S yr^{-1} after the optimization. The new simulated total budget is almost balanced (−4 to −17 Gg S yr^{-1}).

We note that the sink flux reduction is mostly driven by a constant reduction of 30 % of our soil uptake of OCS, therefore always reaching its minimal allowed value. The leaf uptake of OCS is also reduced up to the limit when starting with the GPP from the LPJ and the ORC models. On average, vegetation and soil optimized uptakes are respectively converging around 840±329 and 335±21 Gg S yr^{-1} (where the uncertainty is defined as one SD of the prior flux range) (Table 2).

The optimization procedure also reduced the other sources (−30 % for anoxic soils and −10 % for anthropogenic emissions).

Our three final sets of optimized fluxes (Table 2) confirm that: (i) large direct emissions of OCS by the tropical oceans, with global annual mean around 845 Gg S yr^{-1} (after optimization), and (ii) vegetation and soil uptakes respectively around 840 and 33 Gg S yr^{-1} (Table 2) would be required to fit the main temporal and spatial variations of atmospheric OCS. These new estimates are in the upper range of previously published global budgets (Table 1).

3.3.3 Optimization of the annual means

Figure 10 presents the prior and optimized annual mean OCS mixing ratios at all stations as a function of the latitude. The improvements, through the optimization, are summarized with the mean RMSE across all sites (see values in the legend). Posterior RMSEs are similar between the three scenarios (around 24) and the reduction between the prior and the posterior values are equivalent to 74, 31 and 27 % for ORC, CLM4CN and LPJ respectively. Note that such improvement is much smaller than for the seasonal cycle where RMSE decreases by 82, 19 and 65 %, respectively (see Fig. 9). The large reduction on average for the soil and leaf uptakes through the op-

ACPD
14, 27663–27729, 2014

timization scheme (see summary in Table 2) thus help reduce the spatial gradients between stations. For example, the simulated difference between SPO and CGO stations in the Southern Hemisphere drops from 10–25 to 2–10 ppt in closer agreement with the observations (around 1 ppt).

4 Discussion

Although our revised OCS budgets agree relatively well with the observed temporal and spatial gradients recorded at NOAA stations (using the LMDz transport model), remaining biases exists. These biases will be first discussed to highlight potential errors in the OCS leaf, soil and ocean surface fluxes. In a second step, we will review and discuss the constraint brought by OCS on the GPP of the three tested DGVMs, when the information from both OCS and CO_2 tracers are combined.

4.1 Simulated atmospheric OCS concentrations: remaining biases

The standard optimizations ("OPTIM_H-Er") using the three DGVMs provide an equilibrated atmospheric budget, with fluxes for the three most important OCS surface processes converging to similar values (Table 2). Global leaf and soil annual uptake decrease to values around 840 and 330 $Gg\,S\,yr^{-1}$ respectively, while the ocean flux remains roughly unchanged at 764 $Gg\,S\,yr^{-1}$ on average across all simulations. These values are much larger than those proposed initially by Kettle et al. (2002) and relatively close to the recent budget calculated by Berry et al. (2013). Large gross surface fluxes are needed to simulate the observed seasonal peak-to-peak amplitude at mid/high latitudes of the Northern Hemisphere (around 120 ppt), as highlighted by the optimizations. Note that the study of Berry et al. (2013) further emphasizes the need for large land surface uptake (leaf and soil) if we are to simulate the observed vertical profiles over vegetated areas (especially the observed drawdown of OCS concentrations in boundary layers; see their Fig. 9). On average our ensemble of tests highlights

ACPD
14, 27663–27729, 2014

for all three scenarios that: (i) uptake through leaves (following GPP) controls the atmospheric seasonal cycle, and (ii) uptake by oxic soils, although the second largest sink, has a limited impact on the atmospheric OCS seasonal cycle.

We summarize below the performances of different optimization scenarios (based on the three DGVMs) and highlight the remaining discrepancies in terms of simulated trend, amplitude and phase of the seasonal cycle. Figure 11 displays the observed minus modeled trend at MLO (first row), the mean square error (MSE) decomposition (phase, bias and variance; see Sect. 2.5, Eq. 3) obtained from the detrended concentrations at ALT and MLO (second and third row) and the amplitude of the seasonal cycle at ALT and MLO (last two rows). The results from several optimization scenarios (based on the three DGVMs) are displayed including prior fluxes ("Pri"), optimized fluxes with high and low uncertainties ("OPTIM_H-Er" and "OPTIM_L-Er"), and three tests where only the leaf, soil or ocean component are optimized (the other components being fixed).

4.1.1 Atmospheric trend

As shown in Fig. 11, the optimization successfully allowed for corrections to the annual trends, for most scenarios. General features are:

1. For ORC, the initial large negative trend can be corrected only if the leaf uptake is decreased by 30 %, which is not possible in the L-Er test. This suggests that LRUs provided by Seibt et al. (2010) could be overestimated and would support using lower LRUs, such as published in other studies (Sandoval-Soto et al., 2005; Stimler et al., 2012; Berkelhammer et al., 2013). Lower LRU values also correspond to the case in Seibt et al. (2010) where the internal mesophyll conductance is set as the major limitation in the diffusional pathway of OCS (global LRU equals 2. 08 on average with this assumption, instead of 2. 8 as used in the present paper). Several studies have focused on estimating the relative uptake of OCS compared to CO_2 by the leaves. However, some studies have shown that OCS-to-GPP uptake

ACPD
14, 27663–27729, 2014

ratio could be plant-specific (Sandoval-Soto et al., 2005; Campbell et al., 2008; Seibt et al., 2010; Stimler et al., 2012; Berkelhammer et al., 2013) and even, under certain conditions, that some plants can release some of the absorbed OCS (Xu et al., 2002; Geng et al., 2006; White et al., 2010). Therefore, recent estimates of the vegetation uptake are still largely uncertain and differ by up to a factor of six (Xu et al., 2002; Kettle et al., 2002; Sandoval-Soto et al., 2005; Berry et al., 2013).

2. Optimizing only one component is usually enough to correct the trend, except for ORC, pointing out again the possibly too large leaf uptake, which might be due to overestimated LRU or too large GPP.

4.1.2 Phase of the atmospheric seasonal cycles

Looking at the phase component of the MSE decomposition to analyze the phase mismatches between simulated and observed OCS concentrations, the general features are:

- On average, only small changes are observed at most sites between prior and the different posterior estimates (only shown for MLO and ALT, Fig. 11, second and third rows). A 35 % reduction of the phase error is noticed at MLO for ORC and also a 25 % improvement for LPJ.
- These small phase changes arise because only a global annual scalar for each flux component is optimized.
- On average, ORC provides, after optimization, the best phase agreement with the observations at high latitude stations of the Northern Hemisphere (shown for ALT); At MLO the optimized results are closer between the three models, although LPJ and CLM4CN provide slightly better matches with the observations (51 and 41 ppt^2 error respectively, versus 70 ppt^2 for ORC).

ACPD
14, 27663–27729, 2014

– Most changes are due to the optimization of the leaf uptake, while "OPTIM_SOIL_ONLY" and "OPTIM_OCEAN_ONLY" configurations do not allow for any significant phase improvement.

– Further improvement of the phase should account for potential variations of LRU through the season, or possible important soil deposition velocity changes through the season, as mentioned in the recent paper by Maseyk et al. (2014). This could be achieved with an optimization of the monthly flux of each component.

4.1.3 Amplitude of the atmospheric seasonal cycles

The diagnosis of the amplitude of the simulated atmospheric OCS levels correspond to the last two rows of Fig. 11, but is also partly revealed by the variance term of the MSE decomposition. Main features are:

– The improvement compared with the prior is mainly induced by the optimization of the OCS leaf uptake.

– Smaller or negligible changes are noticed at ALT and MLO stations when only the ocean fluxes are optimized ("OPTIM_OCEAN_ONLY" configuration), but significant improvements can be seen at southernmost stations (10 % variance error correction, not shown).

– When only the soil uptake is optimized ("OPTIM_SOIL_ONLY" configuration), no improvement on the simulated amplitude is obtained.

– The amplitude is too large in the prior for ORC at both ALT and MLO and remains too large at ALT after optimization, suggesting that either LRU values or GPP fluxes are too large for high latitude ecosystems. LPJ provides the best compromise in terms of amplitude when we consider all stations. However, the optimization of only one global coefficient for each flux does not allow for corrections of

ACPD
14, 27663–27729, 2014

local flux biases, which leads to over- and under-estimated amplitudes at different sites for both LPJ and ORC.

- For CLM4CN, the simulated amplitude is too small at most stations, and is not corrected through the optimization. This poor improvement is due to the initial phase mismatch that cannot be corrected with the optimization of a global scaling factor.

- Finally, one should note that the amplitude of the atmospheric signal also depends on the transport model and potential vertical mixing errors. The LMDz version that is used is believed to have too large a mixing in the planetary boundary layer (PBL) (Patra et al., 2011; Locatelli et al., 2013), which would thus dampened the amplitude of the seasonal cycle.

4.1.4 Annual mean atmospheric spatial gradients

We used the bias diagnosis from the MSE decomposition, which also accounts for any remaining trend mismatch, to analyze the annual mean gradients. As demonstrated by the results of the optimization of only one component ("OPTIM_XXX_ONLY" tests), all processes make a similar impact on the annual mean OCS concentrations. However, the optimization scheme leads to a degradation of the bias error at MLO for the three models and the bias remains highly variable at other sites. The constraint imposed by the global mean on the simulation through the optimization scheme is not providing a significant correction. We should also note that the overall fit at some stations can be decreased (see for instance CLM4CN at MLO, Fig. 11) when the optimized set of surface flux scalars lead to compensation by improvements at other sites.

4.2 Joint constraint of OCS and CO_2 cycles to correct the GPP seasonal cycle

There is increasing debate about the usefulness of possible parallel optimization of OCS (influenced by photosynthesis and microbiological activity in the soil) and CO_2

ACPD
14, 27663–27729, 2014

(mostly influenced by photosynthesis and respiration) and the added information retrieved by using both tracers. We now analyze and discuss potential constraints on the GPP of each ecosystem model that could be derived from the results of the OCS simulations (direct and inverse) and of additional CO_2 simulations (see methods Sect. 2.5). Figures 5 and 6 display in the righthand columns the atmospheric CO_2 concentrations simulated with the net CO_2 ecosystem exchange (NEE = GPP – Respiration) from the three DGVMs used for the OCS scenarios (including also fossil fuel emissions and ocean fluxes). Figure 5 compares the smoothed temporal variations of the simulated CO_2 and OCS concentrations at three stations (ALT, MLO and SPO). For CO_2, all three models capture the observed seasonal cycle with nevertheless significant biases in terms of amplitude and/or phase, depending on the DGVM. As first described by Montzka et al. (2007), the OCS seasonal patterns are similar to CO_2, but with noticeable differences in the timing of the maximum and minimum. The largest difference is observed at the SPO station with a phase shift of nearly five months between the two tracers. Additionally, Fig. 6 quantifies the contribution of the leaf uptake and of the GPP to the total simulated concentrations, for OCS and CO_2, respectively. In the Northern Hemisphere, the phase and amplitude of the OCS seasonal cycle is primarily driven by the OCS leaf uptake, while for CO_2 the seasonal cycle combines both GPP and respiration fluxes. Our OCS modeling framework thus provides support for a new constraint on GPP. Note, however, that for OCS, the other flux components (mainly the soil uptake and the ocean release) also contribute to the seasonal cycle but with nearly canceling effects.

We now discuss the implications of the simulated OCS and CO_2 biases for each DGVM, separately. We refer to Fig. 12 that displays the normalized amplitude of the simulated OCS seasonal cycle as a function of the normalized amplitude of the simulated CO_2 seasonal cycle at all stations (the normalization is done with respect to the observations).

ACPD
14, 27663–27729, 2014

4.2.1 ORC

The analysis of the concentrations at boreal stations provides a first hint on northern high latitude ecosystems. We observe that both OCS and CO_2 simulated seasonal amplitude are too large at ALT (by factors 2 and 1.5, respectively). While the sole CO_2 diagnosis would suggest either too large GPP during boreal summer or too small amplitude of the respiration seasonal cycle, the additional OCS diagnosis indicates that the GPP of ORC is indeed too large for high latitude ecosystems. For OCS, uncertainties in LRU values also contribute to the model data mismatch. As suggested by Berkelhammer et al. (2013) the LRUs from Seibt et al. (2010) are on the upper range of the different estimates published so far (+30 % compared to the mean estimates). However, a 30 % reduction of the LRU that corresponds to the optimized fluxes of the "INV_H-Er" case (see Table 3) still produces an amplitude of the seasonal cycle at ALT larger than the observation by a factor 1.3 (Fig. 12). Such remaining discrepancy thus confirms potential over-estimation of the ORC GPP. Note that for both tracers the phase of the seasonal cycle is relatively well captured (Fig. 5).

The signal at MLO integrates the contribution from the land (and ocean) fluxes of the whole Northern Hemisphere. In this case, there is a relatively good agreement for the phase and amplitude of the CO_2 seasonal cycle, while for OCS the amplitude is still too large (by a factor of 1.5). This suggests that the chosen LRU values are indeed too large and that the too large GPP for boreal ecosystems, noticed above, may be compensated by too small GPP at mid and low latitudes. The result of the standard optimization leads to the right amplitude at MLO, which further indicates that the 30 % global reduction of OCS leaf uptake is sufficient on average to compensate for too high GPP at northern ecosystems and potentially too large LRU.

The seasonal cycle at the remote SPO station is more difficult to interpret as (i) the amplitude of the cycle is 8 times smaller than at MLO for CO_2 and (ii) all surfaces fluxes (i.e. from leaf, soil, and ocean) have a shared contribution to the overall seasonal

ACPD
14, 27663–27729, 2014

cycle. The too large amplitude of ORC for CO_2 reflects discrepancies in both GPP and respiration fluxes, but also in air–sea exchanges.

Overall, the joint OCS/CO_2 analysis points towards discrepancies in the ORC GPP, with large overestimated values at high latitudes in the Northern Hemisphere. Such conclusion directly corroborates the results obtained by Kuppel et al. (2014), using the same ecosystem model, when optimizing its parameters with eddy-covariance flux measurements (CO_2 and latent heat flux). They proposed a large reduction of the GPP for boreal broadleaf and boreal needleleaf forests.

4.2.2 CLM4CN

The amplitude of the seasonal cycle simulated with CLM4CN is underestimated at nearly all stations for both OCS and CO_2, with a modeled-to-observed ratio between 0.6 and 0.9, except at CGO where the amplitude is overestimated (Fig. 12). Moreover, as evidenced in Fig. 5, the phase shift in the OCS seasonal cycle at boreal stations (i.e., ALT) also occurs for CO_2, with an earlier drawdown of the modeled concentrations compared to the observation (around two months). Such phase shift is much smaller or close to zero at temperate and low latitude stations of the Northern Hemisphere.

The combined OCS and CO_2 discrepancies point toward biases in the CLM4CN simulated gross carbon fluxes. First, the GPP of high northern latitude ecosystems is most likely out of phase, with a too strong increase of photosynthesis in spring. Using only the CO_2 tracer would suggest that one or both gross carbon fluxes are out of phase (photosynthesis and respiration). The benefit of the OCS tracer is to clearly point toward GPP as the major source of discrepancies, given that for OCS the leaf uptake, which is proportional to GPP, drives the overall seasonal cycle (see Fig. 6). Second, the amplitude of the GPP is also most likely underestimated for most ecosystems. While the CO_2 concentrations do not permit us to blame the GPP more than the respiration, the OCS points again towards too small a GPP during the peak of the growing season.

Increasing by 20 % and shifting by two month the seasonal course of the CLM4CN GPP for high latitudes would create a significant improvement of both OCS and CO_2

ACPD
14, 27663–27729, 2014

simulated concentrations. At SPO, the CO_2 seasonal cycle is in good agreement with the observations, while the OCS seasonal cycle shows too large an amplitude and an earlier maximum – similarly with the two other DGVMs. These features are more difficult to interpret given the shared contribution of land and ocean fluxes.

4.2.3 LPJ

Using the GPP from LPJ leads to intermediary results for the seasonal amplitude, for both tracers, with no systematic biases across stations (Fig. 12).

If we consider boreal stations, the modeled seasonal amplitude for CO_2 is 20 % lower than the observations, while for OCS it is 50 % higher. As noticed above, the temporal variation of the OCS concentrations at these sites is slightly out of phase with a too early a drawdown in spring. This would suggest that the increase of the GPP of boreal ecosystems in spring is too early and too strong in LPJ (see for instance Fig. A4 in the Supplement). However, to match both OCS and CO_2 atmospheric signals, this would also require a change in the temporal variation of the ecosystem respiration flux in order to fit the CO_2 signal.

If we consider the whole Northern Hemisphere, using the MLO records, the phase shift becomes much lower for OCS. The too low amplitude for CO_2 would suggest that either the GPP is underestimated during the peak of the growing season (it is much smaller than when using ORC, see Fig. A4) or that the respiration is too large during summer time. The OCS diagnostic with slightly too large an amplitude at MLO (Fig. 5) suggests that: (i) the main bias comes from the respiration, and (ii) the LRU values from Seibt et al. (2010) are likely overestimated (as already pointed out), which would explain the larger amplitude for OCS. As can be seen in Fig. A4, the LPJ model is the only one with respiration fluxes of the same magnitude as the GPP fluxes, in temperate regions of the Northern Hemisphere, in the mid and late summer. Reducing the intensity of the respiration fluxes during this period would allow for larger annual variations of the CO_2 mixing ratios, more consistent with the observations while still keeping the correct GPP-based representation of the OCS leaf uptake for the model.

ACPD
14, 27663–27729, 2014

Overall, the above joint OCS and CO_2 analysis points towards deficiencies for each model's gross carbon fluxes. Although these deficiencies are coherent between the three models, such as the decrease of ORC GPP for temperate and high latitude ecosystems which would bring it closer to LPJ and CLM4 estimates, or to shift the phase of CLM4CN (and partly LPJ) GPP for high northern ecosystems, some caution is still needed before drawing firm conclusions. For instance we should further investigate:

- The impact of potential atmospheric transport errors. Indeed the mixing within atmospheric transport model is still subject to significant uncertainties (Ref), which in turn may impact the conclusions that are directly linked to the amplitude of the seasonal cycle. Nonetheless, the LMDz model has been used in many tracer transport studies with no strong known biases (Peylin et al., 2014).
- The seasonality of soil OCS uptake. Our modeling strategy, based on similarities between H_2 and OCS uptake by soils, leads to a relatively small seasonal cycle of the OCS soil flux. Any further modifications of the seasonality of that component would directly impact our conclusions and to a certain extent our diagnostic on the gross carbon fluxes of the three DGVMs.
- The representation of LRU values which could describe the amplitude of the OCS seasonal cycle, through seasonal variations of the OCS-to-CO_2 uptake ratio values. More recent estimates based on additional in situ measurements are likely to provide lower LRU values than those of Seibt et al. (2010). LRU values have also been proved to vary depending on available light, and therefore to change according to seasons (Maseyk et al., 2014).

5 Conclusions

Several studies have proposed a relationship between GPP and a concomitant OCS uptake by the vegetation, which would partly explain the atmospheric OCS concentra-

ACPD
14, 27663–27729, 2014

tion variations, yet the observed atmospheric measurements of OCS concentrations have never been used in a quantitative way to obtain information about the GPP of current global vegetation models. In this context, this study proposed, a new set of global sources and sinks of OCS, using the GPP from three different global vegetation models to compute the leaf uptake of OCS. We further used the LMDz atmospheric transport model to compute the temporal and spatial gradients of OCS (as well as of CO_2) observed in the atmosphere.

We achieved the representation of a global OCS budget fully based on parameterized processes that include large emissions by the ocean and important uptake by soil and vegetation, After optimization of all flux components within given ranges of uncertainty, a new flux scenario matches the observed OCS trend in the atmosphere (close to zero). The model OCS gradients are in good agreement with the observations in terms of seasonal amplitude and phase of the seasonal cycle, and in terms of spatial variations of the annual mean concentrations. Data from the Northern Hemisphere stations of the NOAA network showed that the GPP-related uptake of OCS mainly controls the seasonal cycle of atmospheric OCS concentrations, with much smaller influence from ocean and soil fluxes.

More importantly, combining the information from OCS and CO_2 atmospheric observations allowed us to highlight potential biases in the GPP of the three dynamic global vegetation models that were used. We showed that: (i) for the ORCHIDEE model, the terrestrial gross carbon fluxes in the Northern Hemisphere high latitudes are currently too large, (ii) for the CLM4CN model, the GPP is out of phase with an uptake of carbon by northern high latitude ecosystems that occurs too early in spring, and (iii) for the LPJ model, the respiration fluxes might be too large during the peak of the growing season on average in the Northern Hemisphere.

For the first time, our study quantifies the potential of OCS measurements to benchmark gross carbon fluxes from current DGVMs. It also highlights the need to better characterize the different processes that control the surface OCS fluxes and in partic-

ACPD
14, 27663–27729, 2014

ular the seasonality of soil uptake. From such preliminary study, we foresee additional and complementary experiments that would:

- Improve the inversion framework in order to optimize the temporal pattern of each flux component, using for instance a monthly time step optimization. This would provide further information on the potential biases associated to the seasonal variations of the GPP of each model.
- Combine the different models for the GPP-related uptake of OCS within a single inversion framework, where we would optimize a unique set of LRU coefficients (for each PFT) together with the GPP fluxes of all DGVMs simultaneously.
- Optimize multi-data streams, based on both atmospheric OCS and CO_2 data. This would allow separate optimization of GPP and respiration, using prior estimates from a given ecosystem model. Optimizing for both tracers would allow us to account for uncertainties associated with the different components of the CO_2 and OCS budgets in the atmosphere simultaneously, relying on the GPP as a shared component.

The Supplement related to this article is available online at doi:10.5194/acpd-14-27663-2014-supplement.

Acknowledgements. Special thanks are due to the National Oceanic and Atmospheric Administration (NOAA)/Global Monitoring Division (GMD) in Boulder, CO for providing the observational data used in this study. We are equally grateful to Elliott Campbell for sharing the flux estimates from Kettle et al. (2002) and to Samuel Elvis for letting us use their global dynamic vegetation model NCAR-CLM4 to compare with the two other models.

ACPD
14, 27663–27729, 2014

References

Barnes, I., Becker, K. H., and Patroescu, I.: The tropospheric oxidation of dimethyl sulfide: a new source of carbonyl sulfide, Geophys. Res. Lett., 21, 2389–2392, 1997.

Beer, C., Reichstein, M., Tomelleri, E., Ciais, P., Jung, M., Carvalhais, N., and Papale, D.: Terrestrial gross carbon dioxide uptake: global distribution and covariation with climate, Science, 329, 834–838, 2010.

Belviso, S., Nguyen, B. C., and Allard, P.: Estimate of carbonyl sulfide (OCS) volcanic source strength deduced from OCS/CO_2 ratios in volcanic gases, Geophys. Res. Lett., 13, 133–136, 1986.

Belviso, S., Masotti, I., Tagliabue, A., Bopp, L., Brockmann, P., Fichot, C., and Fukuchi, M.: DMS dynamics in the most oligotrophic subtropical zones of the global ocean, Biogeochemistry, 110, 215–241, 2012.

Belviso, S., Schmidt, M., Yver, C., Ramonet, M., Gros, V., and Launois, T.: Strong similarities between nighttime deposition velocities of carbonyl sulphide and molecular hydrogen inferred from semi-continuous atmospheric observations in Gif-sur-Yvette, Paris region, Tellus B, 65, 20719, doi:10.3402/tellusb.v65i0.20719, 2013.

Berkelhammer, M., Asaf, D., Still, C., Montzka, S., Noone, D., Gupta, M., and Yakir, D.: Constraining surface carbon fluxes using in situ measurements of carbonyl sulfide and carbon dioxide, Global Biogeochem. Cy., 28, 161–179, 2014.

Berry, J., Wolf, A., Campbell, J. E., Baker, I., Blake, N., Blake, D., and Zhu, Z.: A coupled model of the global cycles of carbonyl sulfide and CO_2: a possible new window on the carbon cycle, J. Geophys. Res.-Biogeo., 118, 842–852, 2013.

Bonan, G. B. and Levis, S.: Quantifying carbon-nitrogen feedbacks in the Community Land Model (CLM4), Geophys. Res. Lett., 37, L07401, doi:10.1029/2010GL042430, 2010.

Bousquet, P., Ringeval, B., Pison, I., Dlugokencky, E. J., Brunke, E.-G., Carouge, C., Chevallier, F., Fortems-Cheiney, A., Frankenberg, C., Hauglustaine, D. A., Krummel, P. B., Langenfelds, R. L., Ramonet, M., Schmidt, M., Steele, L. P., Szopa, S., Yver, C., Viovy, N., and Ciais, P.: Source attribution of the changes in atmospheric methane for 2006–2008, Atmos. Chem. Phys., 11, 3689–3700, doi:10.5194/acp-11-3689-2011, 2011.

Campbell, J. E., Carmichael, G. R., Chai, T., Mena-Carrasco, M., Tang, Y., Blake, D. R., and Stanier, C. O.: Photosynthetic control of atmospheric carbonyl sulfide during the growing season, Science, 322, 1085–1088, 2008.

ACPD
14, 27663–27729, 2014

Carouge, C., Bousquet, P., Peylin, P., Rayner, P. J., and Ciais, P.: What can we learn from European continuous atmospheric CO_2 measurements to quantify regional fluxes – Part 1: Potential of the 2001 network, Atmos. Chem. Phys., 10, 3107–3117, doi:10.5194/acp-10-3107-2010, 2010a.

Carouge, C., Rayner, P. J., Peylin, P., Bousquet, P., Chevallier, F., and Ciais, P.: What can we learn from European continuous atmospheric CO_2 measurements to quantify regional fluxes – Part 2: Sensitivity of flux accuracy to inverse setup, Atmos. Chem. Phys., 10, 3119–3129, doi:10.5194/acp-10-3119-2010, 2010b.

Chevallier, F., Feng, L., Bösch, H., Palmer, P. I., and Rayner, P. J.: On the impact of transport model errors for the estimation of CO_2 surface fluxes from GOSAT observations, Geophys. Res. Lett., 37, L21803, doi:10.1029/2010GL044652, 2010.

Chin, M. and Davis, D. D.: Global sources and sinks of OCS and CS2 and their distributions, Global Biogeochem. Cy., 7, 321–337, 1993a.

Chin, M. and Davis, D. D.: A reanalysis of carbonyl sulfide as a source of stratospheric background sulfur aerosol, J. Geophys. Res.-Oc. Atm., 100, 8993–9005, 1993b.

Chin, M., Rood, R. B., Lin, S. J., Müller J. F., and Thompson, A. M.: Atmospheric sulfur cycle simulated in the global model GOCART: model description and global properties, J. Geophys. Res.-Oc. Atm., 105, 24671–24687, 2000.

Ciais, P., Reichstein, M., Viovy, N., Granier, A., Ogée, J., Allard, V., and Valentini, R.: Europe-wide reduction in primary productivity caused by the heat and drought in 2003, Nature, 437, 529–533, 2005.

Constant, P., Chowdhury, S. P., Pratscher, J., and Conrad, R.: Streptomycetes contributing to atmospheric molecular hydrogen soil uptake are widespread and encode a putative high-affinity [NiFe]-hydrogenase, Environ. Microbiol., 12, 821–829, 2010.

Conway, T. J., Tans, P. P., Waterman, L. S., Thoning, K. W., Kitzis, D. R., Masarie, K. A., and Zhang, N.: Evidence for interannual variability of the carbon cycle from the National Oceanic and Atmospheric Administration/Climate Monitoring and Diagnostics Laboratory global air sampling network, J. Geophys. Res.-Atmos., 99, 22831–22855, 1994.

Geng, C. and Mu, Y.: Carbonyl sulfide and dimethyl sulfide exchange between trees and the atmosphere, Atmos. Environ., 40, 1373–1383, 2006.

Grace, J. and Rayment, M.: Respiration in the balance, Nature, 404, 819–820, 2000.

ACPD
14, 27663–27729, 2014

Hauglustaine, D. A., Brasseur, G. P., Walters, S., Rasch, P. J., Müller, J. F., Emmons, L. K., and Carroll, M. A.: MOZART, a global chemical transport model for ozone and related chemical tracers: 2. Model results and evaluation, J. Geophys. Res.-Atmos., 103, 28291–28335, 1998.
Hourdin, F., Musat, I., Bony, S., Braconnot, P., Codron, F., Dufresne, J. L., and Lott, F.: The LMDZ4 general circulation model: climate performance and sensitivity to parametrized physics with emphasis on tropical convection, Clim. Dynam., 27, 787–813, 2006.
Kato, H., Saito, M., Nagahata, Y., and Katayama, Y.: Degradation of ambient carbonyl sulfide by Mycobacterium spp. in soil, Microbiology+, 154, 249–255, 2008.
Kesselmeier, J., Teusch, N., and Kuhn, U.: Controlling variables for the uptake of atmospheric carbonyl sulfide by soil, J. Geophys. Res.-Atmos., 104, 11577–11584, 1999.
Kettle, A. J., Kuhn, U., Von Hobe, M., Kesselmeier, J., and Andreae, M. O.: Global budget of atmospheric carbonyl sulfide: temporal and spatial variations of the dominant sources and sinks, J. Geophys. Res.-Atmos., 107, 4658, doi:10.1029/2002JD002187, 2002.
Kloster, S., Feichter, J., Maier-Reimer, E., Six, K. D., Stier, P., and Wetzel, P.: DMS cycle in the marine ocean-atmosphere system – a global model study, Biogeosciences, 3, 29–51, doi:10.5194/bg-3-29-2006, 2006.
Knohl, A., Werner, R. A., Brand, W. A., and Buchmann, N.: Short-term variations in δ13C of ecosystem respiration reveals link between assimilation and respiration in a deciduous forest, Oecologia, 142, 70–82, 2005.
Koch, D., Jacob, D., Tegen, I., Rind, D., and Chin, M.: Tropospheric sulfur simulation and sulfate direct radiative forcing in the Goddard Institute for Space Studies general circulation model, J. Geophys. Res.-Oc. Atm., 104, 23799–23822, 1999.
Kottek, M., Grieser, J., Beck, C., Rudolf, B., and Rubel, F.: World map of the Köppen-Geiger climate classification updated, Meteorol. Z., 15, 259–263, 2006.
Krinner, G., Viovy, N., de Noblet-Ducoudré, N., Ogée, J., Polcher, J., Friedlingstein, P., and Prentice, I. C.: A dynamic global vegetation model for studies of the coupled atmosphere–biosphere system, Global Biogeochem. Cy., 19, GB1015, doi:10.1029/2003GB002199, 2005.
Kobayashi, K. and Salam, M. U.: Comparing simulated and measured values using mean squared deviation and its components, Agron. J., 92, 345–352, 2000.
Kuppel, S., Peylin, P., Maignan, F., Chevallier, F., Kiely, G., Montagnani, L., and Cescatti, A.: Model–data fusion across ecosystems: from multi-site optimizations to global simulations, Geosci. Model Dev. Discuss., 7, 2961–3011, doi:10.5194/gmdd-7-2961-2014, 2014.

ACPD
14, 27663–27729, 2014

Lasslop, G., Reichstein, M., Papale, D., Richardson, A. D., Arneth, A., Barr, A., and Wohlfahrt, G.: Separation of net ecosystem exchange into assimilation and respiration using a light response curve approach: critical issues and global evaluation, Glob. Change Biol., 16, 187–208, 2010.

Launois, T., Belviso, S., Bopp, L., Fichot, C. G., and Peylin, P.: A new model for the global biogeochemical cycle of carbonyl sulfide – Part 1: Assessment of direct marine emissions with an oceanic general circulation and biogeochemistry model, Atmos. Chem. Phys. Discuss., 14, 20677–20720, doi:10.5194/acpd-14-20677-2014, 2014.

Lawrence, D. M. and Swenson, S. C.: Permafrost response to increasing Arctic shrub abundance depends on the relative influence of shrubs on local soil cooling versus large-scale climate warming, Environ. Res. Lett., 6, 045504, doi:10.1088/1748-9326/6/4/045504, 2011.

Locatelli, R., Bousquet, P., Chevallier, F., Fortems-Cheney, A., Szopa, S., Saunois, M., Agusti-Panareda, A., Bergmann, D., Bian, H., Cameron-Smith, P., Chipperfield, M. P., Gloor, E., Houweling, S., Kawa, S. R., Krol, M., Patra, P. K., Prinn, R. G., Rigby, M., Saito, R., and Wilson, C.: Impact of transport model errors on the global and regional methane emissions estimated by inverse modelling, Atmos. Chem. Phys., 13, 9917–9937, doi:10.5194/acp-13-9917-2013, 2013.

Lorimer, G. H. and Pierce, J.: Carbonyl sulfide: an alternate substrate for but not an activator of ribulose-1, 5-bisphosphate carboxylase, J. Biol. Chem., 264, 2764–2772, 1989.

Marland, G., Brenkert, A., and Olivier, J.: CO_2 from fossil fuel burning: a comparison of ORNL and EDGAR estimates of national emissions, Environ. Sci. Policy, 2, 265–273, 1999.

Maseyk, K., Berry, J. A., Billesbach, D., Campbell, J. E., Torn, M. S., Zahniser, M., and Seibt, U.: Sources and sinks of carbonyl sulfide in an agricultural field in the Southern Great Plains, P. Natl. Acad. Sci. USA, 111, 9064–9069, 2014.

Montzka, S. and Tans, P.: Can carbonyl sulfide help constrain gross vegetative fluxes of carbon dioxide?, AGU Fall Meeting Abstracts, American Geophysical Union, Fall Meeting 2004, abstract #B21E-04, 2004AGUFM.B21E..04M, 1, 4 pp., 2004.

Montzka, S. A., Calvert, P., Hall, B. D., Elkins, J. W., Conway, T. J., Tans, P. P., and Sweeney, C.: On the global distribution, seasonality, and budget of atmospheric carbonyl sulfide (COS) and some similarities to CO_2, J. Geophys. Res.-Oc. Atm., 112, D09302, doi:10.1029/2006JD007665, 2007.

ACPD
14, 27663–27729, 2014

Morfopoulos, C., Foster, P. N., Friedlingstein, P., Bousquet, P., and Prentice, I. C.: A global model for the uptake of atmospheric hydrogen by soils, Global Biogeochem. Cy., 26, GB3013, doi:10.1029/2011GB004248, 2012.

Nguyen, B. C., Mihalopoulos, N., Putaud, J. P., and Bonsang, B.: Carbonyl sulfide emissions from biomass burning in the tropics, J. Atmos. Chem., 22, 55–65, 1995.

Patra, P. K., Houweling, S., Krol, M., Bousquet, P., Belikov, D., Bergmann, D., Bian, H., Cameron-Smith, P., Chipperfield, M. P., Corbin, K., Fortems-Cheiney, A., Fraser, A., Gloor, E., Hess, P., Ito, A., Kawa, S. R., Law, R. M., Loh, Z., Maksyutov, S., Meng, L., Palmer, P. I., Prinn, R. G., Rigby, M., Saito, R., and Wilson, C.: TransCom model simulations of CH_4 and related species: linking transport, surface flux and chemical loss with CH_4 variability in the troposphere and lower stratosphere, Atmos. Chem. Phys., 11, 12813–12837, doi:10.5194/acp-11-12813-2011, 2011.

Peylin, P., Chevallier, F., and Engelen, R.: The contribution of AIRS data to the estimation of CO_2 sources and sinks, Geophys. Res. Lett., 32, L23801, doi:10.1029/2005GL024229, 2005.

Peylin, P., Bacour, C., MacBean, N., Leonard, S., Maignan, F., Thum, T., and Santaren, D.: How best to optimize a global process-based carbon land surface model?, EGU General Assembly Conference Abstracts, Vol. 16, 10302 pp., 2014.

Piovesan, G. and Adams, J. M.: Carbon balance gradient in European forests: interpreting EUROFLUX, J. Veg. Sci., 11, 923–926, 2000.

Poulter, B., Ciais, P., Hodson, E., Lischke, H., Maignan, F., Plummer, S., and Zimmermann, N. E.: Plant functional type mapping for earth system models, Geosci. Model Dev., 4, 993–1010, doi:10.5194/gmd-4-993-2011, 2011.

Poulter, B., Frank, D., Ciais, P., Myneni, R. B., Andela, N., Bi, J., and Van der Werf, G. R.: Contribution of semi-arid ecosystems to interannual variability of the global carbon cycle, Nature, 509, 600–603, 2014.

Protoschill-Krebs, G. and Kesselmeier, J.: Enzymatic pathways for the Consumption of Carbonyl Sulphide (COS) by higher plants, Bot. Acta, 105, 206–212, 1992.

Protoschill-Krebs, G., Wilhelm, C., and Kesselmeier, J.: Consumption of carbonyl sulphide by Chlamydomonas reinhardtii with different activities of carbonic anhydrase (CA) induced by different CO_2 growing regimes, Bot. Acta, 108, 445–448, 1995.

Protoschill-Krebs, G., Wilhelm, C., and Kesselmeier, J.: Consumption of carbonyl sulphide (COS) by higher plant carbonic anhydrase (CA), Atmos. Environ., 30, 3151–3156, 1996.

ACPD
14, 27663–27729, 2014

Reichstein, M., Falge, E., Baldocchi, D., Papale, D., Aubinet, M., Berbigier, P., and Valentini, R.: On the separation of net ecosystem exchange into assimilation and ecosystem respiration: review and improved algorithm, Glob. Change Biol., 11, 1424–1439, 2005.

Sandoval-Soto, L., Stanimirov, M., von Hobe, M., Schmitt, V., Valdes, J., Wild, A., and Kesselmeier, J.: Global uptake of carbonyl sulfide (COS) by terrestrial vegetation: Estimates corrected by deposition velocities normalized to the uptake of carbon dioxide (CO_2), Biogeosciences, 2, 125–132, doi:10.5194/bg-2-125-2005, 2005.

Sandoval-Soto, L., Kesselmeier, M., Schmitt, V., Wild, A., and Kesselmeier, J.: Observations of the uptake of carbonyl sulfide (COS) by trees under elevated atmospheric carbon dioxide concentrations, Biogeosciences, 9, 2935–2945, doi:10.5194/bg-9-2935-2012, 2012.

Scartazza, A., Mata, C., Matteucci, G., Yakir, D., Moscatello, S., and Brugnoli, E.: Comparisons of $\delta^{13}C$ of photosynthetic products and ecosystem respiratory CO_2 and their responses to seasonal climate variability, Oecologia, 140, 340–351, 2004.

Schaphoff, S., Lucht, W., Gerten, D., Sitch, S., Cramer, W., and Prentice, I. C.: Terrestrial biosphere carbon storage under alternative climate projections, Climatic Change, 74, 97–122, 2006.

Schenk, S., Kesselmeier, J., and Anders, E.: How does the exchange of one oxygen atom with sulfur affect the catalytic cycle of carbonic anhydrase?, Chem.-Eur. J., 10, 3091–3105, 2004.

Scherr, N. and Nguyen, L.: Mycobacterium versus Streptomyces – we are different, we are the same, Curr. Opin. Microbiol., 12, 699–707, 2009.

Seibt, U., Wingate, L., Lloyd, J., and Berry, J. A.: Diurnally variable δ18O signatures of soil CO_2 fluxes indicate carbonic anhydrase activity in a forest soil, J. Geophys. Res.-Biogeo., 111, G04005, doi:10.1029/2006JG000177, 2006.

Seibt, U., Kesselmeier, J., Sandoval-Soto, L., Kuhn, U., and Berry, J. A.: A kinetic analysis of leaf uptake of COS and its relation to transpiration, photosynthesis and carbon isotope fractionation, Biogeosciences, 7, 333–341, doi:10.5194/bg-7-333-2010, 2010.

Simmons, J. S., Klemedtsson, L., Hultberg, H., and Hines, M. E.: Consumption of atmospheric carbonyl sulfide by coniferous boreal forest soils, J. Geophys. Res.-Atmos., 104, 11569–11576, 1999.

Sitch, S., Smith, B., Prentice, I. C., Arneth, A., Bondeau, A., Cramer, W., and Venevsky, S.: Evaluation of ecosystem dynamics, plant geography and terrestrial carbon cycling in the LPJ dynamic global vegetation model, Glob. Change Biol., 9, 161–185, 2003.

ACPD
14, 27663–27729, 2014

Smith-Downey, N. V., Randerson, J. T., and Eiler, J. M.: Temperature and moisture dependence of soil H_2 uptake measured in the laboratory, Geophys. Res. Lett., 33, L14813, doi:10.1029/2006GL026749, 2006.
Stimler, K., Montzka, S. A., Berry, J. A., Rudich, Y., and Yakir, D.: Relationships between carbonyl sulfide (COS) and CO_2 during leaf gas exchange, New Phytol., 186, 869–878, 2010.
Suntharalingam, P., Kettle, A. J., Montzka, S. M., and Jacob, D. J.: Global 3-D model analysis of the seasonal cycle of atmospheric carbonyl sulfide: implications for terrestrial vegetation uptake, Geophys. Res. Lett., 35, L19801, doi:10.1029/2008GL034332, 2008.
Tarantola, A.: Inverse Problems Theory, Methods for Data Fitting and Model Parameter Estimation, Elsevier, Southampton, 1987.
Takahashi, T., Sutherland, S. C., Wanninkhof, R., Sweeney, C., Feely, R. A., Chipman, D. W., and De Baar, H. J.: Climatological mean and decadal change in surface ocean pCO_2, and net sea–air CO_2 flux over the global oceans, Deep-Sea Res. Pt. II, 56, 554–577, 2009.
van der Werf, G. R., Randerson, J. T., Giglio, L., Collatz, G. J., Mu, M., Kasibhatla, P. S., Morton, D. C., DeFries, R. S., Jin, Y., and van Leeuwen, T. T.: Global fire emissions and the contribution of deforestation, savanna, forest, agricultural, and peat fires (1997–2009), Atmos. Chem. Phys., 10, 11707–11735, doi:10.5194/acp-10-11707-2010, 2010.
Van Diest, H. and Kesselmeier, J.: Soil atmosphere exchange of carbonyl sulfide (COS) regulated by diffusivity depending on water-filled pore space, Biogeosciences, 5, 475–483, doi:10.5194/bg-5-475-2008, 2008.
Wania, R., Ross, I., and Prentice, I. C.: Implementation and evaluation of a new methane model within a dynamic global vegetation model: LPJ-WHyMe v1.3.1, Geosci. Model Dev., 3, 565–584, doi:10.5194/gmd-3-565-2010, 2010.
Whelan, M. E., Min, D. H., and Rhew, R. C.: Salt marsh vegetation as a carbonyl sulfide (COS) source to the atmosphere, Atmos. Environ., 73, 131–137, 2013.
White, M. L., Zhou, Y., Russo, R. S., Mao, H., Talbot, R., Varner, R. K., and Sive, B. C.: Carbonyl sulfide exchange in a temperate loblolly pine forest grown under ambient and elevated CO_2, Atmos. Chem. Phys., 10, 547–561, doi:10.5194/acp-10-547-2010, 2010.
Wingate, L., Seibt, U., Maseyk, K., Ogée, J., Almeida, P., Yakir, D., and Mencuccini, M.: Evaporation and carbonic anhydrase activity recorded in oxygen isotope signatures of net CO_2 fluxes from a Mediterranean soil, Glob. Change Biol., 14, 2178–2193, 2008.

ACPD
14, 27663–27729, 2014

Wingate, L., Ogée, J., Burlett, R., Bosc, A., Devaux, M., Grace, J., and Gessler, A.: Photosynthetic carbon isotope discrimination and its relationship to the carbon isotope signals of stem, soil and ecosystem respiration, New Phytol., 188, 576–589, 2010.

Wöhlfahrt, G., Brilli, F., Hörtnagl L., Xu, X., Bingemer, H., Hansel, A., and Loreto, F.: Carbonyl sulfide (COS) as a tracer for canopy photosynthesis, transpiration and stomatal conductance: potential and limitations, Plant Cell Environ., 35, 657–667, 2012.

Xu, X., Bingemer, H. G., Georgii, H. W., Schmidt, U., and Bartell, U.: Measurements of carbonyl sulfide (COS) in surface seawater and marine air, and estimates of the air–sea flux from observations during two Atlantic cruises, J. Geophys. Res.-Oc. Atm., 106, 3491–3502, 2001.

Yi, Z., Wang, X., Sheng, G., Zhang, D., Zhou, G., and Fu, J.: Soil uptake of carbonyl sulfide in subtropical forests with different successional stages in south China, J. Geophys. Res.-Atmos., 112, D08302, doi:10.1029/2006JD008048, 2007.

ACPD
14, 27663–27729, 2014

Table 1. Summary of forward and inverse simulations performed using the LMDz transport model and specific setups of surface fluxes. We compared three dynamic global vegetation models (DGVMs), carried out a series of sensitivity tests and optimized major fluxes (the allowed range of variations is expressed in %). ORC stands for ORCHIDEE. CLM4CN stands for NCAR-CLM4. v_{H_2} and v_{OCS} are the deposition velocities of H_2 and OCS.

		Simulations names	OCS leaf uptake[1]	OCS uptake by oxic soil[2]	OCS oceanic emissions
FORWARD	MODEL	STD_ORC	GPP from ORC	v_{H_2} map (Morfopoulos et al., 2012)	Direct: Launois et al. (2014)
RUNS	INTER-COMPARISON			v_{OCS}/v_{H_2} = 0.75	Indirect from DMS: Masotti et al. (2014) Indirect from CS_2: Kettle et al. (2002)
		STD_CLM4CN	GPP from CLM4CN	"	"
		STD_LPJ	GPP from LPJ	"	"
	SENSITIVITY TESTS	TEST_Ocean_±30	GPP from ORC	"	Increased/Decreased by 30 %
		TEST_Soil_MORF_0.5:1	"	v_{H_2} map (Morfopoulos et al., 2012) v_{OCS}/v_{H_2} = 0.5 (H. Chen, personal communication, 2013)	Direct: Launois et al. (2014) Indirect from DMS: Masotti et al. (2014) Indirect from CS_2: Kettle et al. (2002)
		TEST_Soil_MORF_1:1	"	v_{H_2} map (Morfopoulos et al., 2012) v_{OCS}/v_{H_2} = 1 (Belviso et al., 2013)	"
		TEST_Soil_BOUSQ_0.5:1	"	v_{H_2} map (Bousquet et al., 2011) v_{OCS}/v_{H_2} = 0.5 (H. Chen, personal communication, 2013)	"
		TEST_Soil_BOUSQ_1:1		v_{H_2} map (Bousquet et al., 2011) v_{OCS}/v_{H_2} = 1 (Belviso et al., 2013)	"
OPTIMIZATION	OPTIM_H-Er	±30 %	±30 %	−30/ + 50 %	
	OPTIM_L-Er	±10 %	±10 %	±10 %	
	OPTIM_LEAF_ONLY	±30 %	±10 %	±10 %	
	OPTIM_SOIL_ONLY	±10 %	±30 %	±10 %	
	OPTIM_OCEAN_ONLY	±10 %	±10 %	−30/ + 50 %	

[1] LRUs from Seibt et al. (2010) are used in all simulations, sensitivity tests and optimizations.
[2] Note that the OCS emissions by anoxic soils were kept unchanged between the simulations, and attributed a ±30 % variation range in all optimization configurations.
All other surface fluxes are either described in the method section or taken directly from Kettle et al. (2002). They are attributed a ±10 % variation range in all optimization configurations.

ACPD
14, 27663–27729, 2014

Table 2. Overview of global budgets of carbonyl sulfide. Units are Gg S yr^{-1}. Shaded cells include new estimates which are compared with data from the recent literature. Only fluxes provided by Kettle et al. (2002) and in the present study have been transported using the LMDz model. DGVM stands for dynamic global vegetation models.

	PROCESSES	Kettle et al. (2002)	Montzka et al. (2007)[2]	Suntharalingam et al. (2008)	Berry et al. (2013)	This study		
SINKS	DGVM used	not relevant	not relevant	not relevant	SiB3	ORC	LPJ	CLM4CN
	Plant uptake	−238	−1115	−490	−738	−1335	−1069	−930
	Soil uptake (oxic soils)	−130	−130	−130	−355		−510	
	Destruction by OH radicals	−120	−120	−120	−101		−100	
	Total sinks	−488	−1365	−740	−1194	−1945	−1679	−1540
SOURCES								
	Anoxic soils and wetlands	26	26	26	neglected		101	
	Direct oceanic emissions of OCS	39	39	230	639[3]		813	
	Indirect oceanic emissions of OCS (from DMS)	156	156		156		133	
	Indirect oceanic emissions of OCS (from CS_2)	81	81		81*		81	
	Direct anthropogenic emissions of OCS	64	64	180	64*		64	
	Indirect anthropogenic emissions of OCS (from DMS and CS_2)	116	116		116		116	
	Biomass burning	38	106	70[1]	136[4]		70	
	Total sources	552	588	506	1192		1379	
	Net total	64	−776	−234	1	−566	−300	−161

[1] Modification to Kettle et al. (2002): biomass burning data are from the total flux of Nguyen et al. (1995).
[2] Median fluxes taken from Montzka et al. (2007) as (max – min)/2.
[3] To provide a balanced global budget of OCS, Berry et al. (2013) increased the marine emissions of Kettle et al. (2002) by 600 Gg S yr^{-1}.
[4] An upper estimate supposedly taken from Kettle et al. (2002) and consistent with the new estimates of Montzka et al. (2007).
* As proposed by Kettle et al. (2002) but incorrectly reported in Table 1 of Berry et al. (2013).

ACPD
14, 27663–27729, 2014

Table 3. OCS surface fluxes before and after their optimization. Units are $Gg\,S\,yr^{-1}$. DGVM stands for dynamic global vegetation models. All allowed ranges of variation presented here correspond to the "H-Er" case (Table 1).

	PROCESSES	Before optimization upper and lower limits of variation			After optimization adjusted fluxes		
	DGVM	ORC	LPJ	CLM4CN	ORC	LPJ	CLM4CN
SINKS	Plant uptake	[−1736, −935]	[−1390, −0.748]	[−1209, −651]	−935*	−748*	−828
	Soil uptake (oxic soils)		[−700, −330]		−330*	−330*	−330*
	Destruction by OH radicals		[−110, −90]		−110*	−104	−110*
	Total sinks	[−2546, −1355]	[−2200, −1168]	[−2019, −1071]	−1375	−1182	−1268
	Anoxic soils and wetlands		[70, 130]		70*	70*	70*
	Direct oceanic emissions of OCS		[569, 1220]		878	700	715
SOURCES	Indirect oceanic emissions of OCS (from DMS)		[93, 173]		104	93*	118
	Indirect oceanic emissions of OCS (from CS_2)		[57, 105]		84	86	84
	Direct anthropogenic emissions of OCS		[58, 70]		58*	58*	64
	Indirect anthropogenic emissions of OCS (from DMS and CS_2)		[104, 128]		104*	104*	128*
	Biomass burning		[63, 77]		71	74	77*
	Total sources		[1014, 1903]		1369	1182	1255
	Net total	[−1532, 548]	[−1186, 735]	[−1005, 832]	−6	0	−13

* Surface fluxes which, after optimization, have reached the set upper or lower limits of variation.

ACPD
14, 27663–27729, 2014

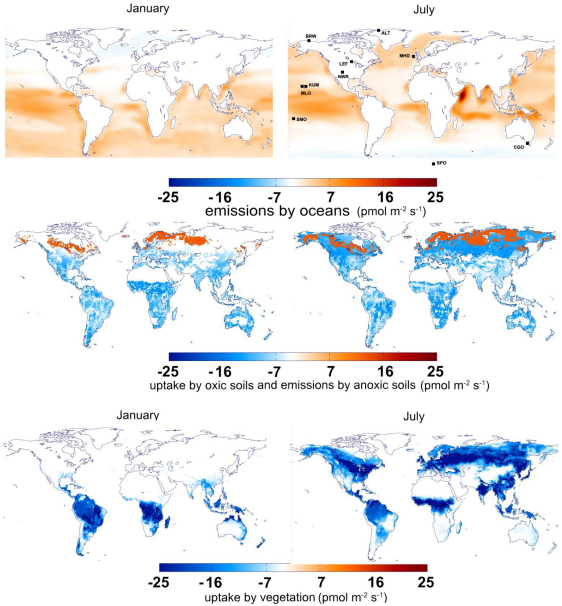

Figure 1. Monthly mean direct oceanic emissions (first row, from the standard run of Launois et al., 2014) for January (left column) and July (right column), monthly mean uptake of OCS by soils (second row, using H_2 deposition velocities (Morfopoulos et al., 2012) and OCS vs. H_2 deposition velocities in a 0.75 : 1 ratio) and vegetation (third row, deduced from the GPP of ORC). The 10 NOAA stations are: SPO, South Pole, 89.9° S, 59° E; CGO, Cape Grim, Australia, 40.7° S, 144.8° E; SMO, American Samoa, 14.3° S, 170.6° W; MLO, Mauna Loa, United States, 19.5° N, 155.6° W; NWR, Niwot Ridge, United States, 40.1° N, 105.6° W; BRW, Barrow, United States, 71.3° N, 156.6° W; ALT, Alert, Canada, 82.5° N, 62.3° W; MHD, Mace Head, Ireland, 53° N, 10° W; KUM, Cape Kumukahi, Hawaii, USA, 19.5° N, 154.8° W and LEF, Wisconsin, United States, 45.6° N, 90.2° W.

ACPD
14, 27663–27729, 2014

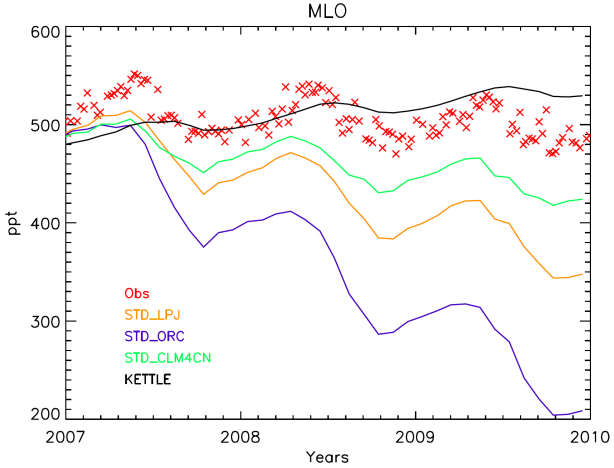

Figure 2. Annual variations of OCS monthly mean mixing ratios (in ppt), simulated and monitored at Mauna Loa. Simulations with the LMDz model use the "STD_ORC", "STD_LPJ" and "STD_CLM4CN" configurations described in Table 1. Data derived solely from the Kettle et al. (2002) surface fluxes are shown in black solid line. Observations (red crosses) are from NOAA-ESRL global monitoring network (Montzka et al., 2007).

ACPD
14, 27663–27729, 2014

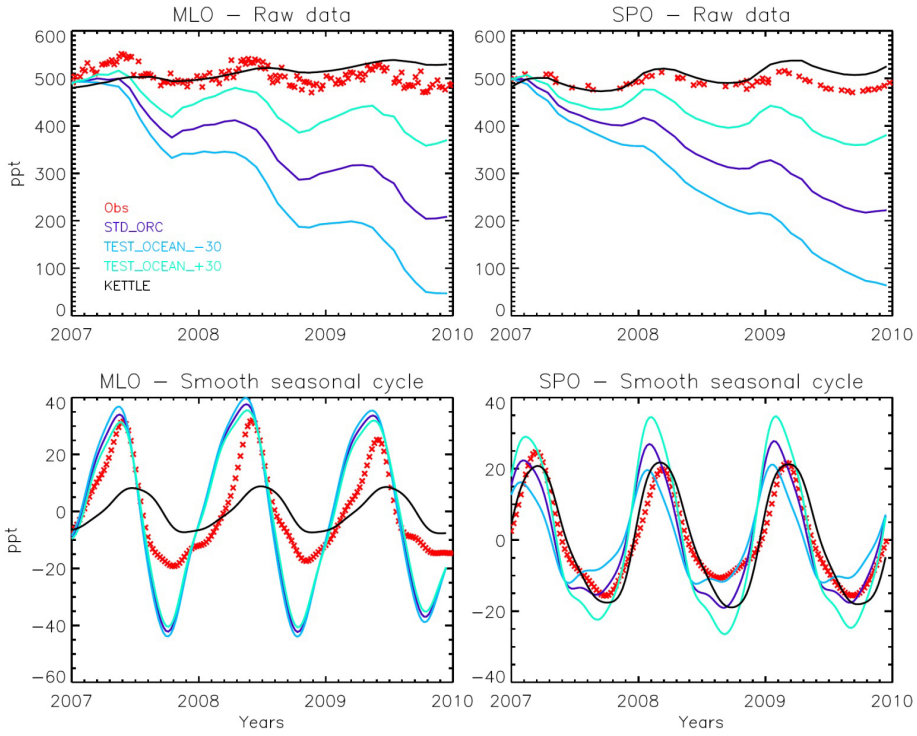

Figure 3. Sensitivity tests performed using the "TEST_Ocean_±30" setup of surface fluxes (Table 1) to simulate the annual variations of OCS monthly mean mixing ratios (upper panels) simulated and monitored at Mauna Loa (left column) and South Pole (right column), and the smoothed seasonal variations obtained after removing the annual trends (lower panels). The simulations based solely on the Kettle et al. (2002) surface fluxes are shown with a black solid line. Observations (red crosses) are from NOAA-ESRL global monitoring network (Montzka et al., 2007).

ACPD
14, 27663–27729, 2014

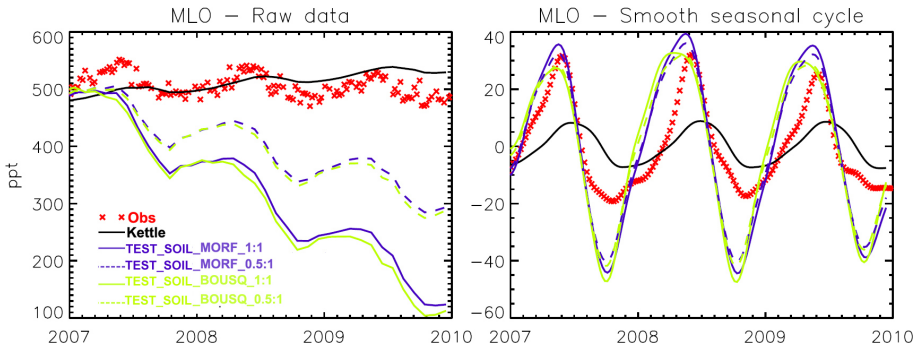

Figure 4. Sensitivity tests performed using the "TEST_Soil_MORF_0. 5:1", "TEST_Soil_MORF_1:1", "TEST_Soil_BOUSQ_0. 5:1" and "TEST_Soil_BOUSQ_1:1" setups of surface fluxes (Table 1) to simulate annual variations of OCS monthly mean mixing ratios (left panel) and smoothed seasonal variations obtained after removing the annual trends (right panel), at Mauna Loa. The simulations based solely on the Kettle et al. (2002) surface fluxes are shown in black solid line. Observations (red crosses) are from NOAA-ESRL global monitoring network (Montzka et al., 2007).

ACPD
14, 27663–27729, 2014

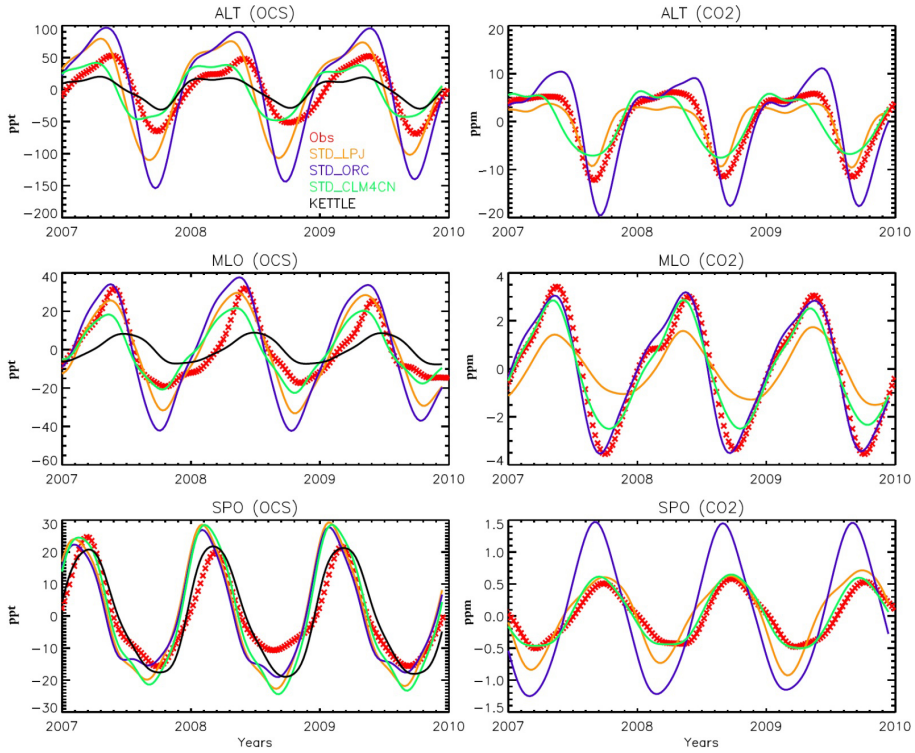

Figure 5. Smoothed seasonal cycles of OCS (left column) and CO_2 (right column) monthly mean mixing ratios, simulated at ALT, MLO and SPO, and obtained after removing the annual trends. Simulations obtained with the LMDz model using the "STD_ORC", "STD_CLM4CN", "STD_LPJ" setups (Table 1). Data derived solely from the Kettle et al. (2002) surface fluxes are shown in black solid line. Observations (red crosses) are from NOAA-ESRL global monitoring network (Montzka et al., 2007).

ACPD
14, 27663–27729, 2014

A new model of the global biogeochemical cycle of carbonyl sulfide – Part 2

T. Launois et al.

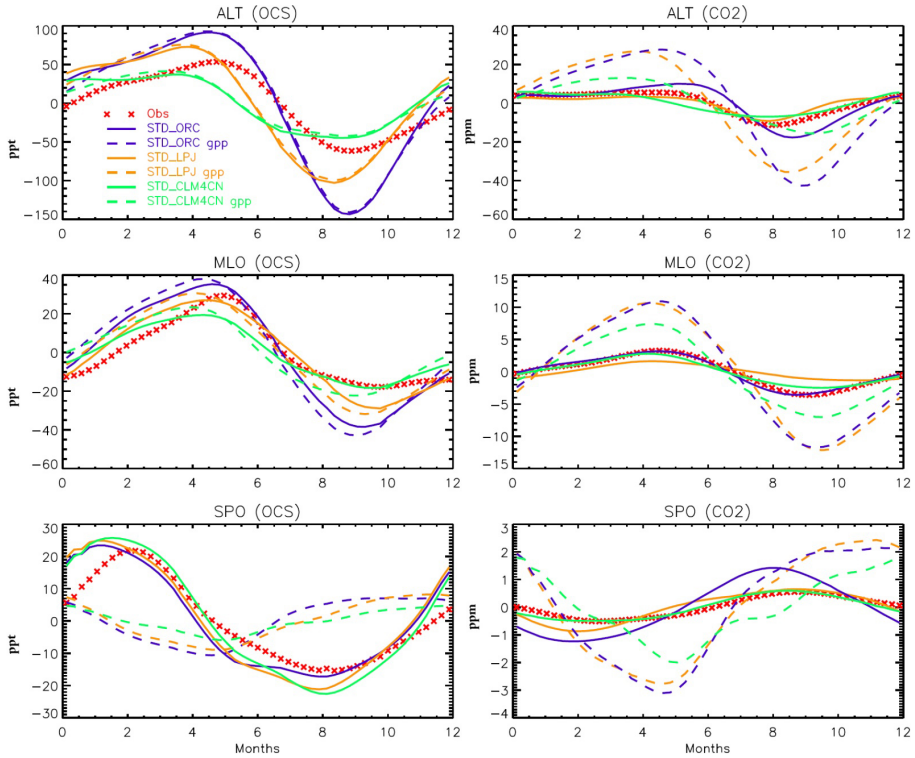

Figure 6. Average smoothed seasonal cycles of OCS (left column) and CO_2 (right column) monthly mean mixing ratios, simulated at ALT, MLO and SPO, and obtained after removing the annual trends. OCS cycles simulated with the LMDz model using the "STD_ORC", "STD_LPJ" and "STD_CLM4CN" setups (Table 1). The dashed lines represent the smoothed seasonal cycles of the OCS (left column) and CO_2 (right column) monthly mean mixing ratios when only the contribution of the leaf OCS uptake (resp. the GPPs) of the three vegetation models are used in the LMDz transport model ("ORC gpp", "CLM4CN gpp" and "LPJ gpp"). Observations (red crosses) are from NOAA-ESRL global monitoring network (Montzka et al., 2007).

ACPD
14, 27663–27729, 2014

A new model of the global biogeochemical cycle of carbonyl sulfide – Part 2

T. Launois et al.

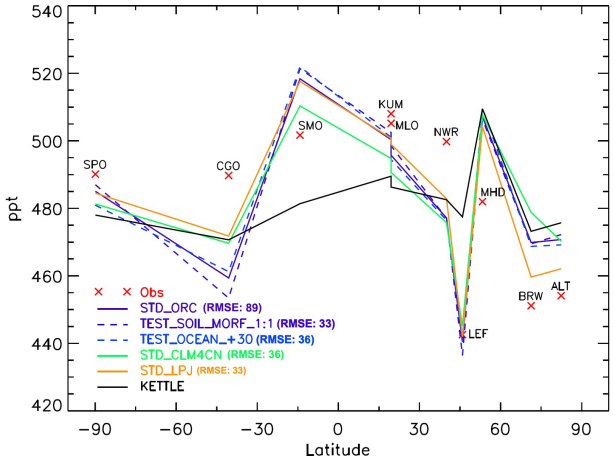

Figure 7. Differences in OCS annual mean mixing ratios between 10 stations of the NOAA monitoring network, plotted as a function of latitude, for observations (red crosses surmounted by station acronyms) and simulations (no symbol). Simulations obtained with the LMDz model using the "STD_ORC", "STD_CLM4CN" and "STD_LPJ" setups (Table 1). Data derived solely from the Kettle et al. (2002) surface fluxes are shown in black solid line. The sensitivity of latitudinal gradients to changes in soil uptake and ocean emissions (dashed colored lines) was investigated using the "TEST_Soil_MORF_1:1+30 %" and "TEST_Ocean_+30 %" setups. Note that the global mean for each mixing ratio series has been set to the global mean of the observations.

ACPD
14, 27663–27729, 2014

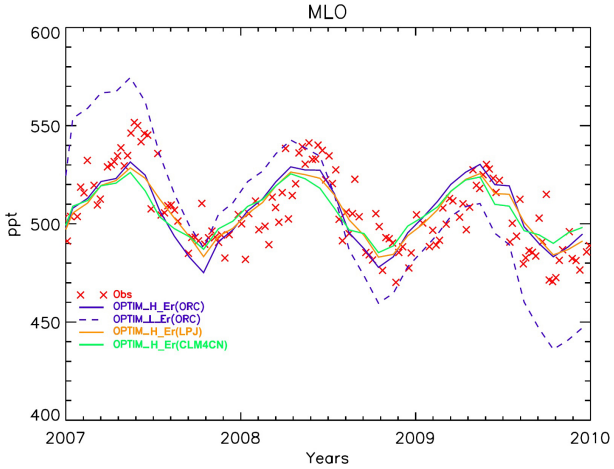

Figure 8. Annual variations of OCS monthly mean mixing ratios (in ppt), optimized and monitored at Mauna Loa. Simulations obtained with the LMDz model using the "OPTIM_H-Er" setup (Table 1) applied to ORC, NCAR-CLM4 and LPJ models. Observations (red crosses) are from NOAA-ESRL global monitoring network (Montzka et al., 2007). A sensitivity test was carried out using ORC and the "OPTIM_L-Er" setup (dashed blue line).

ACPD
14, 27663–27729, 2014

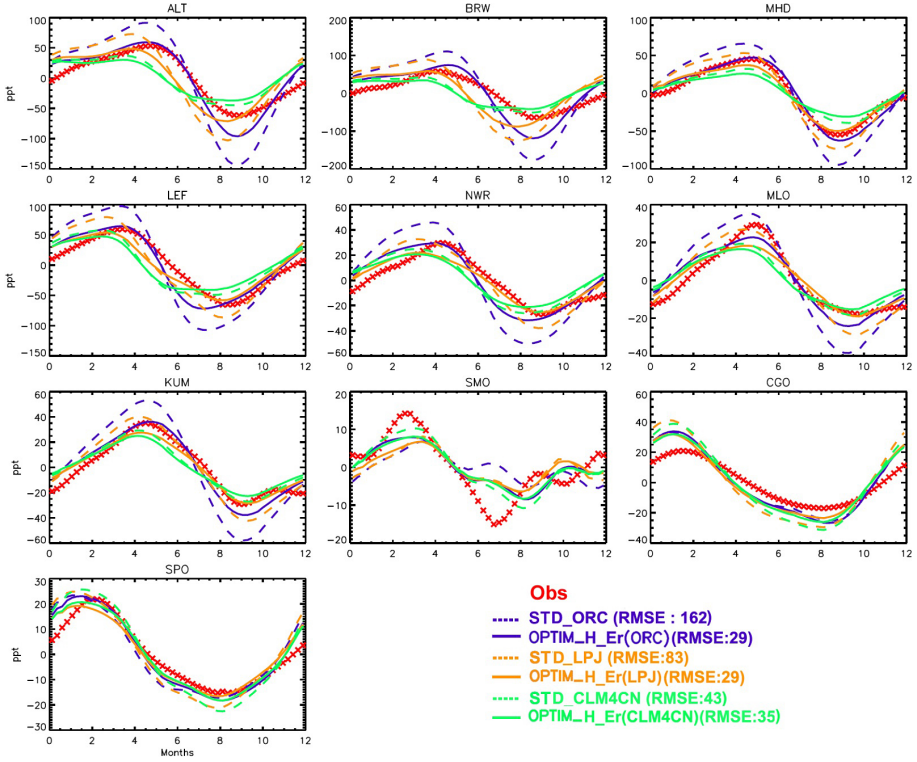

Figure 9. Smoothed seasonal cycles of OCS monthly mean mixing ratios, simulated at 10 stations of the NOAA monitoring network, and obtained after removing the annual trends. Forward simulations with the LMDz model use surface fluxes from the "STD_ORC", "STD_CLM4CN" and "STD_LPJ" setups (dashed lines). The "OPTIM_H-Er" setup (Table 1) was used in the optimizations (solid lines). Observations (red crosses) are from NOAA-ESRL global monitoring network (Montzka et al., 2007). Global root mean square errors (RMSE) are given in the legend.

ACPD
14, 27663–27729, 2014

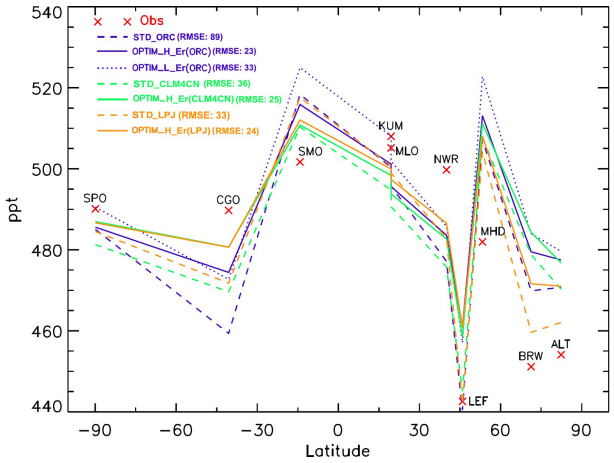

Figure 10. Differences in OCS annual mean mixing ratios between 10 stations of the NOAA monitoring network, plotted as a function of latitude, for observations (red crosses surmounted by station acronyms) and simulations (no symbol, forward approach (colored dashed lines), inverse approach (colored solid lines)). Forward simulations with the LMDz model use the "STD_ORC", "STD_CLM4CN" and "STD_LPJ" setups (dashed lines). The "OPTIM_H-Er" setup (Table 1) was used in the optimizations (solid lines). A sensitivity test was carried out using ORC and the "OPTIM_L-Er" setup (blue dotted line). Note that the global mean for each mixing ratio series has been set to the global mean of the observations.

ACPD
14, 27663–27729, 2014

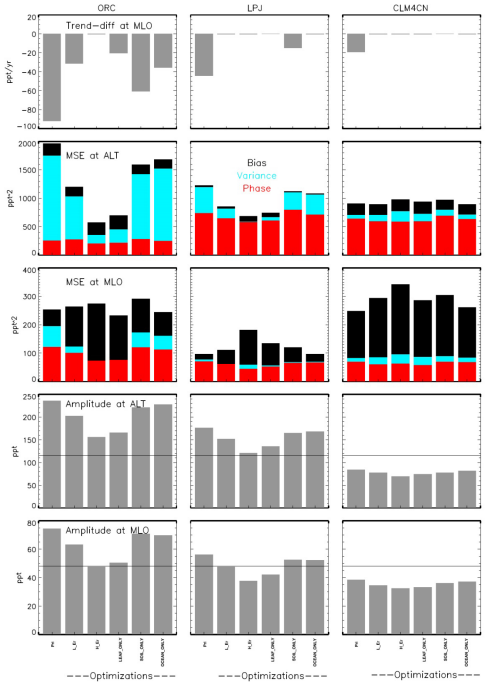

Figure 11. Upper row: differences in annual trends (in $\mathrm{ppt\,yr^{-1}}$) between simulated monthly mean OCS mixing ratios and measurements, at Mauna Loa. Second and third rows: analysis of smoothed seasonal cycles in simulations and observations (at Alert and Mauna Loa, respectively), and calculation of the mean square error (MSE, in $\mathrm{ppt^2}$) decomposed into three components (bias, phase and variance, as described by Kobayashi and Salam, 2000). Fourth and fifth rows: specific analysis of the amplitude of simulated smoothed seasonal cycles, at Alert and Mauna Loa respectively. The bar plots compare the forward approach ("Pri" using the "STD_ORC", "STD_LPJ" or "STD_CLM4CN" setups) to the optimization runs (using the "OPTIM_H_Er", "OPTIM_L_Er", "OPTIM_Leaf_ONLY", "OPTIM_Soil_ONLY" and "OPTIM_Ocean_ONLY" setups, Table 1).

ACPD
14, 27663–27729, 2014

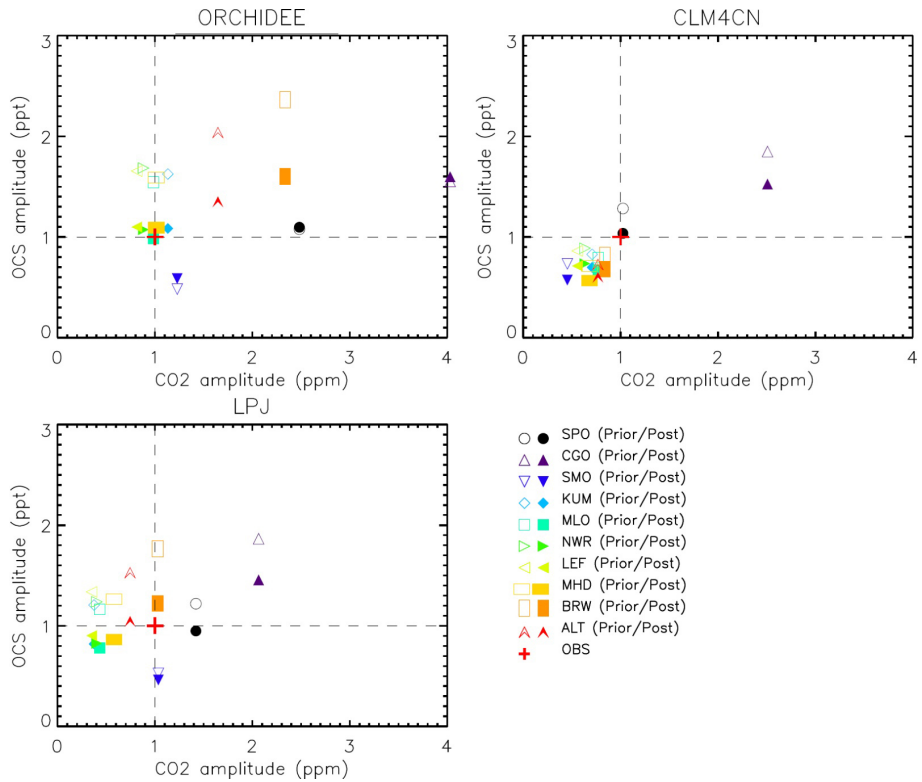

Figure 12. Scatter plots of normalized amplitudes of smoothed seasonal cycles of OCS versus those of CO_2, before and after optimization of OCS fluxes at 10 stations of the NOAA monitoring network, obtained from the "STD_ORC", "STD_CLM4CN" and "STD_LPJ" setups for the forward simulations and the "OPTIM_H-Er" setup for the optimizations, over the period 2006–2010. Since the amplitude of the seasonal cycle in the observations at each site is used to normalize that of the simulations, the normalized amplitude of observations is 1 (red cross). Hence, a linear translation along the y axis towards $y = 1$ characterizes the optimization process.

ACPD
14, 27663–27729, 2014